**Atmospheric
Chemistry
and Physics**

Spatial-temporal variations in surface ozone in Northern China as observed during 2009–2010 and possible implications for future air quality control strategies

G. Tang[1], **Y. Wang**[1], **X. Li**[1], **D. Ji**[1], **S. Hsu**[2], **and X. Gao**[3]

[1]State Key Laboratory of Atmospheric Boundary Layer Physics and Atmospheric Chemistry (LAPC), Institute of Atmospheric Physics, Chinese Academy of Sciences, Beijing 100029, China
[2]National Central University, Taoyuan 32001, Taiwan
[3]Tianjin Environmental Monitoring Center, Tianjin 300191, China

Correspondence to: Y. Wang (wys@dq.cern.ac.cn)

Abstract. The Project of Atmospheric Combined Pollution Monitoring over Beijing and its Surrounding Areas, was an intensive field campaign conducted over Northern China between June 2009 and August 2011 to provide a comprehensive record of ozone (O_3) and nitrogen oxides (NO_x) and contribute to an in-depth understanding of air pollution in Northern China and its driving forces. In this campaign, 25 stations in an air-quality monitoring network provided regional-scale spatial coverage. In this study, we analyzed the data on O_3 and NO_x levels obtained at 22 sites (out of 25 sites due to data availability) over Northern China between 1 September 2009 and 31 August 2010. Our goal was to investigate the O_3 spatial-temporal variations and control strategy in this area. Significant diurnal and seasonal variations were noted, with the highest concentrations typically found at around 03:00 p.m. (local time) and in June. The lowest concentrations were generally found during early morning hours (around 06:00 a.m.) and in December. Compared with July and August, June has increased photochemical production due to decreased cloud cover coupled with reduced O_3 loss due to less dry deposition, inducing an O_3 peak appearing in June. The averaged O_3 concentrations were lower in the plains area compared with the mountainous area due to the titration effects of high NO_x emissions in urban areas. When the characteristics of O_3 pollution in different regions were distinguished by factor analysis, we found high levels of O_3 that exceeded China's National Standard throughout the plains, especially over Beijing and the surrounding areas. An integrated analysis with emissions data, meteorological data, and topography over Northern China found that the meteorological conditions were the main factors that dominated the spatial variations of O_3, with the presence of abundant emissions of precursors in this area. The smog production algorithm and space-based $HCHO/NO_2$ column ratio were used to show the O_3-NO_x-VOCs sensitivity and examine the control strategy of O_3 over Northern China. The results show that summer O_3 production in the plains and northern mountainous areas was sensitive to VOCs and NO_x, respectively. The presented results are intended to provide guidance for redefining government strategies to control the photochemical formation of air pollutants over Northern China and are relevant for developing urban agglomerations worldwide.

1 Introduction

The increase in tropospheric ozone is a serious environmental concern because of its adverse impacts on human health and vegetation (NRC, 1991; POPG, 1997) and the resultant greenhouse effect (Houghton et al., 2001). Photochemical ozone is formed from NO_x and VOCs through non-linear interactions between chemical reactions and meteorology (Seinfeld and Pandis, 1998). The relationship between precursor pollutants and photochemical O_3 differs by location due to the emissions' distribution and meteorology (NRC, 1991).

Elevated O_3 concentrations that range from local to regional scales have been extensively reported (Lee et al., 1998; Oltmans et al., 1998; Jacob et al., 1999; Lin et al., 2000; Broennimann et al., 2002; Akimoto, 2003; Lelieveld et al., 2004; Parrish et al., 2004; Jonson et al., 2005; Zhang et al., 2008; Tang et al., 2009). For example, large, widespread

emission sources in East Asia (Streets et al., 2003; Zhang et al., 2009), especially in China (Li et al., 2010; Huang et al., 2011), have resulted in high concentrations of O_3 precursors, namely NO_x, VOCs, and CO. These precursors have, in turn, led to high levels of oxidants (Zhang et al., 1998; Xu et al., 2008; Zhang et al., 2008; Shao et al., 2009; Tang et al., 2009; Wang et al., 2009; Tang et al., 2010a, b; Wang et al., 2010; Xu et al., 2010, 2011; Wang et al., 2011). Therefore, the increase in Asian continental outflows was suggested to account for an increase in O_3 in the northern Pacific Ocean region (Parrish et al., 2004). Jacob et al. (1999) suggested that the tripling of Asian anthropogenic emissions between 1985 and 2010 would lead to an increase in the monthly mean O_3 concentration by 2–6 ppbv in the western US and by 1–3 ppbv in the eastern US. This type of intercontinental O_3 transport has strong effects on climate (Jacob et al., 1999; Akimoto, 2003). These studies emphasize that the research on O_3 pollution in China will provide benefits for the mitigation of global air pollution.

In recent years, The Beijing-Tianjin-Hebei (BTH) economic circle located in the center of the vibrant economic area of Northern China has become one of the world's fastest developing economic zones (National Bureau of Statistics of China, 2010; Lu et al., 2010). The BTH region consists of 11 cities within the province of Hebei, namely Shijiazhuang, Tangshan, Qinhuangdao, Handan, Xingtai, Baoding, Zhangjiakou, Chengde, Cangzhou, Langfang and Hengshui, plus the Beijing and Tianjin municipalities. Beijing, the political, economic and cultural center of China, has a population of nearly 20 million and 5 million mobile vehicles within an area of $16\,800\,km^2$. Tianjin and Hebei surrounding Beijing, have become China's workshop and a major manufacturing base for items such as oil, steel, cement, electronics, and a range of other heavy industrial products (National Bureau of Statistics of China, 2010). Various anthropogenic emissions, especially motor vehicle exhaust and volatile solvent usage in BTH and industrial emissions in Tianjin and Hebei, have increased significantly and have been transported to impact the air quality within the region. The territory has a complex topography with two sides (northerly and westerly) nestled among the mountains and the other side (southerly) bounded by the North China Plain (Fig. 1). Regarding the typical topography over Northern China, the regional pollution becomes much more evident when southwesterly and southeasterly wind prevails in the BTH region.

Over the past decade, the Beijing municipal government has gradually tightened the regulations (Table S1) to alleviate emissions from automobiles, industrial and domestic sources in this city. The municipal government has implemented the following projects: Air, Water and Soil Environmental Pollution Mechanism and Its Regulates-Control strategy in Beijing and Its Ambient Area (1999–2005); Study on the Countermeasure of Air Pollutant in Beijing (2000–2002) and Strategic Study of Beijing Air Quality Standard
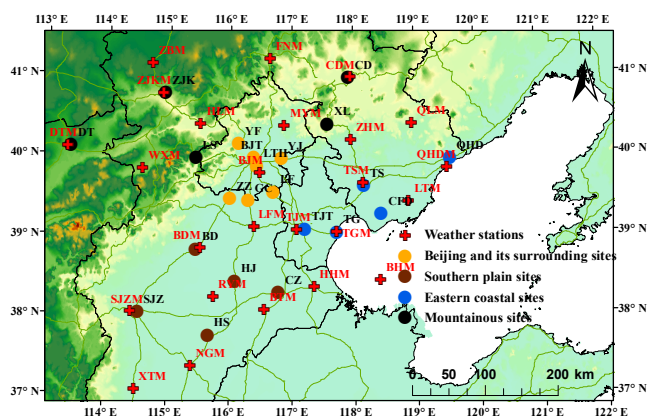

Fig. 1. The Air Quality Network and weather stations over Northern China.

(2003–2005). These measures have produced rapid decrease of pollutants from the burning of coal (Zhang et al, 2006; Lu et al., 2010). However, the increase in population and the number of motor vehicles has induced pollutants from other more complex sources and exhibited different spatial-temporal variations (Zhang et al., 1998; Hao et al., 2005; Chai et al., 2006; Tang et al., 2009). For instance, high levels of various volatile inorganic/organic compounds, photochemical oxidants and particulate matters have been reported for the area (Tang et al., 1995; Xu et al., 2005; Cheng et al., 2007; Chan and Yao, 2008; Xin et al., 2010). Worst of all, in stagnant weather for summer over the BTH region, atmospheric pollutants from various emissions easily accumulate and lead to serious pollution events, exhibiting decreased visibility, high concentration of particulate matter and ozone in the region (Ying et al., 1999; Song et al., 2002; Ding et al., 2005). Since 2004, Beijing's local government has realized the importance of regional collaborative prevention and control for air pollutants. In other words, three governments are cooperating to decrease the emissions from various sources in order to abate air pollution and improve the air quality over the BTH region. Therefore, cooperated with other governments and institutes, Beijing local government has implemented 2 projects: study of the Transmission and Transformation of Beijing and its Surrounding Area Air Pollution and the Object of the Beijing Air Quality (2005–2007) and Air quality safeguards Research of Beijing during the 29th Olympic games (2006–2008) for monitoring, evaluating and predicting the air quality of Beijing and its surrounding areas for the 29th Olympic Games. Due to the continuous efforts of three local governments, the emission restrictions were notably successful in improving air quality in Beijing during the Olympics (Wang et al., 2009; Cermak and Knutti, 2009; Xin et al., 2010). However, O_3 pollution in the BTH region outside of Beijing has not yet been investigated adequately; large gaps and uncertainties remain in the

knowledge of characteristics of regional O_3 pollution and its mitigation strategies in BTH. Moreover, to develop effective policies for O_3 pollution control, our understanding of O_3-VOCs-NO_x chemistry over the entire BTH region needs to be improved through more observational and modeling studies.

To further control air pollution in the BTH region over Northern China after the Olympics, the "Project of Atmospheric Combined Pollution Monitoring over Beijing and its Surrounding Areas" was organized by the Chinese Ecosystem Research Network (CERN), the Institute of Atmospheric Physics (IAP), and the Chinese Academy of Sciences (CAS) to provide an in-depth understanding and a comprehensive record of ozone, $PM_{2.5}$, PM_{10}, and other air pollutants in this quickly developing region of China. Extensive spatial coverage was made possible by the participation of 25 air-quality network stations, which provided a comprehensive picture of the ozone pollution on a regional scale.

In this study, we illustrate the spatial-temporal variations of surface ozone and related components over Northern China between September 2009 and August 2010 using data from the air quality monitoring network. Furthermore, a combined approach that incorporates the emissions inventories, meteorological simulations, and topography was used to evaluate the main driving forces of summer O_3 concentrations over Northern China. Finally, based on the smog production algorithm and space-based monthly HCHO and NO_2 column concentrations, the sensitivity of ozone production to its precursors was evaluated to identify strategies for controlling photochemical pollution over Northern China.

2 Methodology

2.1 Air quality network

2.1.1 Sites

The Air Quality Network over Northern China, affiliated with the CAS-IAP-CERN, was expanded based on the established BTH Atmospheric Environment Monitoring Network (Xin et al., 2010) from 17 to 25 sites. The network monitored air pollutants in real-time and provided early warnings of air pollution in the region from June 2009 to August 2011. The network comprises 25 air-quality monitoring stations across this area (Fig. 1). Ambient concentrations of PM_{10}, $PM_{2.5}$, SO_2, NO_2, NO, CO, and O_3 are measured in real-time at each station. Based on geopolitical locations, the network includes five sites in Beijing (BJT, LTH, YF, SQL), four sites in the surrounding Beijing area (GC, ZZ, LF, XH, YJ), five sites in the southern plains (BD, SJZ, HJ, HS, CZ), six sites in the eastern coastal area (QHD, TS, CFD, QA, TJT, TG), three urban sites (ZJK, CD, DT), and two rural sites (XL and LS) in the northwestern mountainous area. All the sites are located remote from specific point emission sources and were

selected to be broadly representative of air pollutant levels for a selected site.

In this study, O_3 and NO_x data from 1 September 2009 through 31 August 2010 were provided by the network. Data quality was carefully evaluated and at all sites the frequency of missing values was checked prior to data analysis. Except for the sites in QA, XH and SQL, which were temporally interrupted during some periods due to network maintenance and upgrading, all other stations have more than 90 % data capture rates for O_3 and NO_x during the one year of monitoring. Therefore, the remaining 22 sites were used to illustrate the spatial-temporal variations over Northern China in this work and the detailed full station names, coordinates and altitude are shown in Table 1.

2.1.2 Measurement techniques

The measurement instruments were housed in a laboratory situated at each site. Ambient air samples were drawn through a 3-m PFA Teflon tube (outside diameter: 12.7 mm; inside diameter: 9.6 mm). The sampling tube inlet was located 1 m above the laboratory, and the outlet was connected to a PFA-made manifold with a bypass pump that drew air at a rate of $15 \, l \, min^{-1}$.

Surface ozone concentrations were measured using a Model 49 i or 49 c ozone analyzer from Thermo Environmental Instruments (TEI), Inc. NO_x levels were measured using the TEI Model 42 C and 42 CTL NO and NO_2 analyzers. The TEI Model 49 i and 49 c detector was found to exhibit a detection limit of 1 ppbv and a precision of 1 ppbv. Both of the NO_x analyzers had a precision of 0.4 ppbv, with the limit of detection for Model 42 C and 42 CTL being 0.4 ppbv and 0.05 ppbv, respectively.

Data quality was evaluated and certified by the China National Accreditation Board of Laboratories (CNAL) and was consistent with international requirements. IAP personnel strictly adhered to national environmental monitoring standards. Quality control checks, including automatic zero-calibration and span checks of gas analyzers, were performed daily, and manual calibrations with standard gases were conducted weekly. The NO_x analyzers were zero-checked and span-checked using a zero gas generator (TEI Model 111) and an internal O_3 source of a multi-gas calibrator (TEI Model 146 C) with a NO standard (National Center for Standard Materials, Beijing, China). Multi-point calibrations of the O_3 analyzer were used as an O_3 calibrator (TEI Model 49 CPS). The sampling methods and instrument protocols as well as quality assurance/quality control (QA/QC) procedures for air quality monitoring are described in detail in the Chinese National Environmental Protection Standard, Automated Methods for Ambient Air Quality Monitoring (HJ/T 193–2005; State Environmental Protection Administration of China, 2006). The measurement techniques are the same as in Tang et al. (2009). The description is repeated here for the reader's convenience.

Table 1. Information on sites and results of factor analysis for daily maximum ozone.

Sites	Longitude	Latitude	Altitude	Factor1	Factor2	Factor3
Baoding (BD)	115.44	38.82	4	0.44	**0.77**	0.29
Beijing (BJT)	116.37	39.97	44	**0.87**	0.33	0.32
Chengde (CD)	117.93	40.97	395	0.43	0.47	0.49
Caofeidian (CFD)	118.44	39.27	11	0.37	0.46	**0.75**
Cangzhou (CZ)	116.78	38.29	12	0.17	**0.64**	0.55
Datong(DT)	113.39	40.09	1058	0.39	0.56	0.31
Gucheng (GC)	116.29	39.44	21	**0.60**	0.64	0.36
Hejian(HJ)	116.08	38.42	66	0.45	**0.63**	0.49
Hengshui (HS)	115.66	37.74	77	0.22	**0.68**	0.40
Langfang (LF)	116.69	39.55	19	**0.69**	0.47	0.48
Lingshan (LS)	115.43	39.97	116	0.23	0.52	0.24
Longtanhu (LTH)	116.43	39.87	31	**0.83**	0.32	0.37
Qinhuangdao (QHD)	119.57	39.95	2	0.40	0.36	**0.61**
Shijiazhuang (SJZ)	114.53	38.03	70	0.47	**0.71**	0.28
Tanggu(TG)	117.72	39.04	13	0.46	0.38	**0.69**
Tianjin (TJT)	117.21	39.08	2	0.37	0.34	**0.69**
Tangshan (TS)	118.16	39.62	14	0.45	0.37	**0.74**
Xinglong (XL)	117.58	40.39	879	0.54	0.46	0.57
Yangfang (YF)	116.13	40.15	78	**0.85**	0.33	0.32
Yanjiao (YJ)	116.82	39.96	26	**0.64**	0.37	0.52
Zhangjiakou (ZJK)	114.92	40.77	777	0.48	0.42	0.36
Zhuozhou (ZZ)	115.99	39.46	48	**0.69**	0.52	0.32

2.2 Data analysis

Several different statistics were utilized to analyze the spatial and temporal characteristics of the measured O_3 and NO_x over Northern China. First, we calculated the maximum, minimum, mean and standard deviations for each site to give us a basic knowledge of weather conditions, O_3 and NO_x variations over Northern China. Second, to examine the shared variance between different sites and identify homogenous ozone clusters, factor analysis was conducted on the daily maximum O_3 as an initial data reduction tool at all 22 sites using the method in Zheng et al. (2010) and Sarnat et al. (2010). Third, Pearson's paired correlation coefficients (R) were calculated as a measure of the linear relationship to illustrate the relative temporal differences between sites. Because correlations alone may not sufficiently depict absolute concentration differences between sites (Pinto et al., 2004), the spatial coefficients of variation (CV) and the coefficients of divergence (COD) of the measured O_3 and NO_x concentrations have been used as Supplement methods to the analysis of correlation, to characterizes the spatial variations of O_3 and NO_x in several multi-site comparative analysis (Wongphatarakul et al., 1998; Pinto et al., 2004; Kim et al., 2005; Cyrys et al., 2008; Krudysz et al., 2008; Sarnat et al., 2010). The CV was averaged over the sampling year and defined as the mean of the standard deviation of the spatial distribution divided by the distribution's mean. The COD was characterized by means of coefficients of divergence (Wongphatarakul

et al., 1998) which are defined as

$$\text{COD}_{fh} = \sqrt{\frac{1}{n}\sum_{i=1}^{n}(\frac{X_{\text{if}} - X_{\text{ih}}}{X_{\text{if}} + X_{\text{ih}}})^2} \quad (1)$$

where X_{if} is the i-th concentration observed at the f-th site, f and h are two monitoring sites, and n is the sample size of observations. The COD of zero indicates the O_3 and NO_x measured at two sites are uniform and a value approaching one means absolute dissimilar or heterogeneity. We use the COD of 0.20 as the threshold to identify the heterogeneity or homogeneity between two sites, which is described in detail in Krudysz et al. (2008). In this context, two sites exhibit strong uniformity with each other in O_3 and NO_x concentrations, showing similar absolute levels, high correlation coefficients, and low CV and COD values.

The summary statistics for each site, including maximum, minimum, mean and standard deviations, were calculated using Microsoft Excel 2003. Factor analysis of the daily maximum O_3 was performed using SPSS 17.0, with varimax rotation, the maximum likelihood extraction method and eigenvalues more than 1.0. The COD of measured O_3 and NO_x were conducted using the statistical software package SAS 9.1 for Windows.

2.3 Model description and experiment design

The Weather Research and Forecasting (WRF, version 3.3) modeling system (Skamarock et al., 2008) was utilized to

simulate the meteorological parameters to illustrate the reasons of the O_3 spatial-temporal variations over Northern China. WRF was run with 28 vertical layers and with the following physics options: the Grell-3D cumulus scheme, the Lin microphysics, unified Noah land-surface model, the Mellor-Yamada-janjic TKE scheme, a rapid radiative transfer model (RRTM) longwave scheme, and Goddard shortwave scheme. Tang et al. (2010b) checked almost all the physics options in WRF comparing to observations and found this setup was most suitable for simulations over Northern China. The National Centers for Environmental Protection (NCEP) 1×1 global reanalysis data and the upper air observation data were used to correct the initial and boundary conditions for the WRF simulations (Fig. S1). The four-dimensional data assimilation (FDDA) technique ("analysis nudging") was used to nudge the temperature, humidity and 3-D winds every 6 h. Hourly meteorological data from WRF was used to calculate the dry deposition of O_3 using version 3.3 of the Meteorology-Chemistry Interface Processor (MCIP) (Byun and Ching, 1999).

WRF was configured to have three domains (Fig. S1). The mother domain with a horizontal grid resolution of 81-km, covered the entire area of China; the 27-km, grid-spacing, inner domain covered Eastern China; and the third domain with 9-km resolution covered Beijing, Tianjin, and Hebei Province. All of the grids had 28 vertical layers extending from the surface to about 15 km above the ground. The vertical layers were unevenly distributed with eight layers in the lowest kilometer, and a surface layer of approximately 38 m. Our WRF simulations were conducted every three and half days from 1 September 2009 to 31 August 2010. To minimize the effect of the initial conditions, we checked the influences of spin-up time and found there was a little difference between half- and one-day spin-up. Therefore, a half-day spin-up was used for each simulation based on former research (Bromwich et al., 2005; Hines and Bromwich, 2008).

Because there were no meteorological data at all air quality monitoring sites, we used data on the China Meteorological Data Sharing Services System website (http://cdc.cma.gov.cn/) for WRF evaluation. Our study area comprised 26 meteorological sites including 2 sites in Beijing, 3 sites in Tianjin, 20 sites in Hebei and 1 site in Shanxi, denoted in Fig. 1 by red crosses and site names with the suffix "M". Predicted meteorological parameters, including temperature, relative humidity, winds and precipitation, were validated against the monthly observations obtained between September 2009 and August 2010 for 26 sites over Northern China. The performance statistics for the WRF calculations were conducted using the Metstat statistical analysis package (Emery et al., 2001).

2.4 O_3-NO_x-VOCs sensitivity diagnosis

2.4.1 The smog production algorithm

The smog production (SP) algorithm was used to examine areas of VOCs and NO_x sensitivity, which qualitatively represented the production of O_3 in smog chambers (Blanchard et al., 1999; Blanchard, 2000), in box model simulations (Blanchard et al., 1999), in air quality model simulations (Blanchard and Stoeckenius, 2001), and in comparison with field measurements (Blanchard and Fairley, 2001). Johnson (1984) and Johnson and Quigley (1989) defined the variable SP as

$$SP(t) = O_3(t) - O_3(0) + NO(0) - NO(t) \qquad (2)$$

All species are represented in units of volume mixing ratio. SP represents the total amount of NO consumed and O_3 produced and is fundamentally associated with the chemical reactions that enable O_3 to accumulate (Blanchard and Fairley, 2001).

The extent of reaction ($E(t) = SP/SP_{max}$) was defined as

$$
\begin{aligned}
E(t) &= \frac{SP(t)}{SP_{max}} \\
&= \frac{O_3(t) + DO_3(t) - O_3(0) + NO(i) - NO(t)}{\beta[NO_x(i)]^\alpha}
\end{aligned}
\qquad (3)
$$

$DO_3(t)$ represents the concentration at time t corresponding to the cumulative mass of ozone lost from time zero to t. This equation required values for the unmeasured quantities $DO_3(t)$, $O_3(0)$, and $NO_x(i)$, which must be estimated from measurements or simulations. We use fixed values of 40 ppbv for $O_3(0)$, 2/3 for α and 19 for β according to Blanchard et al. (1999). $DO_3(t)$, which can also be used to estimate $NO_x(i)$, was estimated using $O_3(t)$, dry deposition velocity ($V_d(t)$) and planetary boundary layer height ($Z(t)$) according to equations specified by Blanchard et al. (1999). Both $V_d(t)$ and $Z(t)$ parameters can be estimated by WRF simulations.

The $E(t)$ represented to what extent a system had proceeded towards its maximum possible O_3 formation (Johnson, 1984; Blanchard and Fairley, 2001), with the transition value of ~0.9 from VOCs-sensitive to NO_x-sensitive regimes. The $E(t)$ thereby indicated the sensitivity of O_3 production to changes in NO_x and VOCs levels at a specific time (Johnson, 1984; Blanchard et al., 1999; Blanchard, 2000; Blanchard and Fairley, 2001). In brief, the box-model and three-dimensional-model calculations indicated that when the $E(t)$ was lower than ~0.6 during the afternoon hours (01:00–04:00 p.m.), the O_3 formation was sensitive to the availability of free radicals rather than NO_x, and O_3 concentrations were positive correlated with VOCs levels (Blanchard and Fairley, 2001). When the $E(t)$ was greater than ~0.8 during the hours of peak O_3, the daily maximum O_3 levels were sensitive to reductions of NO_x concentrations (Blanchard and Fairley, 2001). In addition, the uncertainties of measurements and methodology indicate that $E(t)$ values

between 0.6 and 0.9 should approximately be regarded as indeterminate or transitional (Blanchard and Fairley, 2001).

2.4.2 Space-based observations of tropospheric NO_2 and HCHO

Tropospheric HCHO and NO_2 columns have been globally monitored continuously in the way of solar backscatter observations since the nadir-viewing GOME-2 satellite instrument started operation in 2007. Global coverage was achieved each day with a typical surface spatial resolution of 0.25 degrees by 0.25 degrees, which was sufficient in resolving the regional scale of O_3 pollution episodes. The GOME-2 retrievals are represented in detail in Boersma et al. (2004) for tropospheric NO_2 and Smedt et al. (2009) for HCHO. The vertical columns were obtained by dividing the slant columns by the air mass factors (AMFs) (Palmer et al., 2001) calculated using scattering weights evaluated from radiative transfer calculations performed using the DISORT code (Dahlbeck and Stamnes, 1991). All GOME-2 observations have been filtered to remove observations where local cloud cover exceeded 40 % (Boersma et al., 2004; Smedt et al., 2009). Both the monthly NO_2 and HCHO data are available on the Tropospheric Emission Monitoring Internet Service (TEMIS) website (http://www.temis.nl/index.php).

The HCHO/NO_2 ratio was gradually used to determine the surface O_3-NO_x-VOCs sensitivity, and the uncertainty in the resulting monthly mean ratio is typically less than 25 % (Martin et al., 2004; Duncan et al., 2010). For this work, we used a HCHO/NO_2 ratio < 1 indicating VOCs-sensitive conditions, while HCHO/NO_2 ratio > 2 indicate NO_x-sensitive conditions. HCHO/NO_2 ratios in the range of 1–2 should generally be considered as transition regime (Martin et al., 2004; Duncan et al., 2010; Witte et al., 2011).

3 Results and discussions

3.1 Model evaluation and meteorology over Northern China

In this section, the model results are examined to extend the understanding of the mesoscale structure between September 2009 and August 2010 beyond what can be seen in the more sparse set of observations. Before the specific structures of the numerical solutions are investigated, it is helpful to review briefly the results for the whole year for which the experiment was conducted. Table 2 presents the statistics between monthly observations and simulations of 26 weather stations for surface-layer temperature, relative humidity, wind speed and precipitation using several common measures of statistical skill (Stauffer and Seaman, 1990). The Table shows mean errors (ME), mean absolute errors (MBE), root mean square errors (RMSE), and correlation coefficients (R) for the former four parameters. The Table shows a very low bias in the surface temperatures and

Table 2. Summary of statistics for surface-layer temperature, relative humidity, wind speed and precipitation.

Parameter	ME[a]	MBE[b]	RMSE[c]	R[d]
Temperature (°C)	0.4	1.0	1.3	1.0
Relative humidity (%)	3.6	7.3	9.0	0.7
Wind speed (m s^{-1})	−1.9	1.9	2.1	0.7
Precipitation (mm)	−3.5	20.4	34.2	0.8

[a] Mean errors.
[b] Mean absolutely errors.
[c] Root mean square errors.
[d] Correlation coefficients.

relative humidity, with typical errors (MBE) of only 1.0 °C and 7.3 %, respectively. However, the surface wind speeds are always overestimated by WRF, which shows high biases of −1.9 m s^{-1} and 1.9 m s^{-1} for ME and MBE, respectively. This overestimation is mostly because the winds in the surface layer tend to be influenced by buildings, small-scale (unresolvable) terrain, and other obstacles or heterogeneity, which is a typical characteristic in a mesoscale meteorological model. Table 2 also shows a small MB for the monthly average precipitation, a moderate RMSE and a high correlation of 0.8. All of the comparisons indicated that the WRF performance was well within the typical range of meteorological modeling studies (Hanna and Yang, 2001; Emery et al., 2001).

Beijing and its surrounding area are in a warm temperate zone and have a typical continental monsoon climate with four distinct seasons. Figure 2 shows the monthly average simulated and observed statistics of ambient temperature, relative humidity, wind speed and precipitation for 26 weather stations between September 2009 and August 2010. In order to show the representative meteorological conditions during this time period, we also illustrated the long-term climatology from 1951 to 2010 in Fig. 2. On average, high temperature and relative humidity appeared in summer, and low temperature and relative humidity appeared in winter and spring, respectively. The hottest and the coldest months were found to be July and January, averaging 26.8 °C and −7.5 °C, respectively, while the most humid and the driest months were in August and April, with 73.3 % and 48.4 %, respectively. In other words, even in winter months, the average RH was over 50 %. The wind speed was much higher in spring than that in other seasons, with the highest monthly average appearing in April. The lowest monthly average precipitation was 0.4 mm in December, and the highest was 161.4 mm in August, which was due to a Siberian high and the East Asian summer monsoon circulation, respectively. In addition, the meteorological conditions during 2009 and 2010 were similar to the long-term climatology.

In addition to the aforementioned meteorological parameters, the simulated vector winds and planetary boundary layer
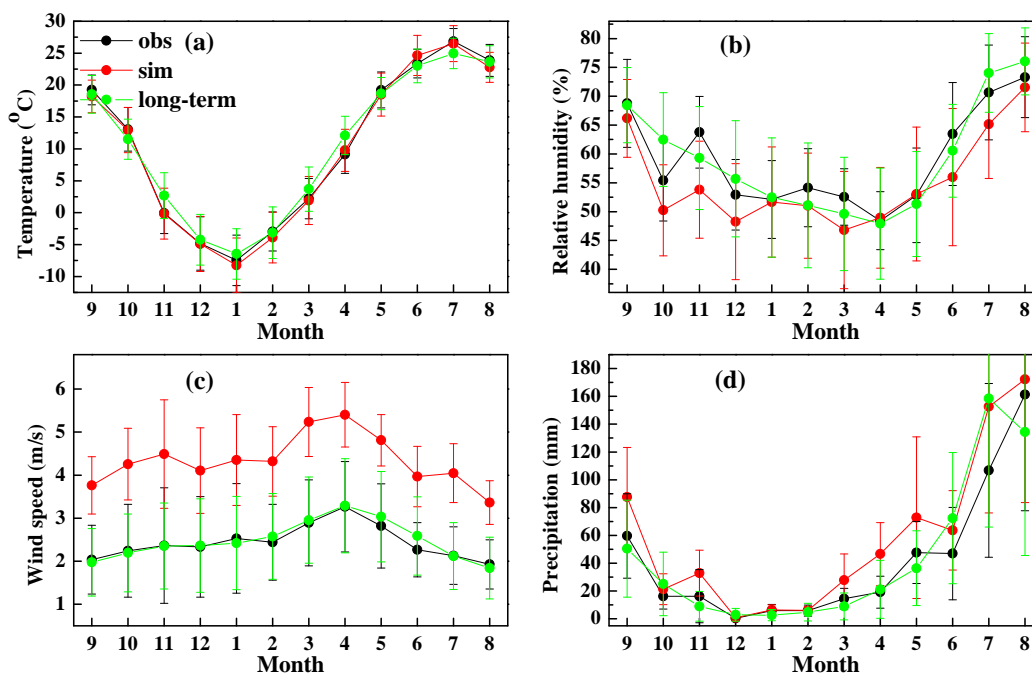
Fig. 2. Simulated and observed monthly variations of temperature **(a)**, relative humidity **(b)**, wind speed **(c)**, and precipitation **(d)**. The values of each species represent averages of measurements and simulations taken from 26 weather stations over Northern China during September 2009 and August 2010, and the values of long-term observations are computed and taken from the same stations during 1951 and 2010.

heights (PBLH) for four seasons between 09:00 and 15:00 were investigated and the results were showed in Fig. 3. The time period is consistent with strong photochemical production of O_3 over the course of the day. During all seasons, the wind speeds were low in the North China Plain and high in mountainous areas. In winter, the northerly and northwesterly winds were much more frequent than that in other seasons. However, the plains and mountainous areas were dominated by southeasterly and southwesterly winds in summer, respectively. In addition, PBLH was highest in spring and lowest in winter. In autumn and spring, PBLH of the plains and mountainous areas had good coincidences. However, PBLH in the plains and mountainous areas showed great differences in winter and summer, whereas PBLH was higher in winter in the plains and in summer in the mountainous areas, respectively. In summary, spring showed a high PBLH and westerly, dry and strong winds; summer had high temperatures, high humidity and southerly weak winds; winter had low temperatures, low PBLH and northwesterly winds; and autumn was similar to spring in temperature, but had characteristically low PBLH, high humidity and northerly weak winds.

3.2 Classification of regional sites and O_3 and NO_x inter-site correlations

In order to classify the regional sites for further analysis, factor analysis (FA) approach was applied to help identify homogenous ozone groups. Table 1 presents the results of the factor analysis for daily maximum ozone (O_{3_max}). Factor analysis conducted on the daily maximum ozone mixing ratio shows that 29.7 % of the variability in the total daily maximum ozone mixing ratio for 7 of the 22 sites was explained by one shared factor; 24.9 % of the variability for 5 of the remaining 15 sites was explained by the second shared factor; and 23.6 % of the variability for 5 of the remaining 10 sites was explained by the third shared factor. Therefore, the FA results showed that the ozone patterns in the BTH region could be classified into four homogenous groups. The first group included 7 sites located in Beijing and its surrounding area with more automobiles and fewer industries, marked with solid orange circles in Fig. 1. The second group consisted of 5 sites located in the southern plains area of the North China Plain, denoted in Fig. 1 by solid brown circles. The third group, marked with solid blue circles in Fig. 1, is composed of 5 sites located east of Beijing and adjacent to the coastline of the Bohai Sea. The second and third groups were characterized by more industries and fewer automobiles compared with the first group, indicating different emissions over three different areas. All of the remaining 5 sites
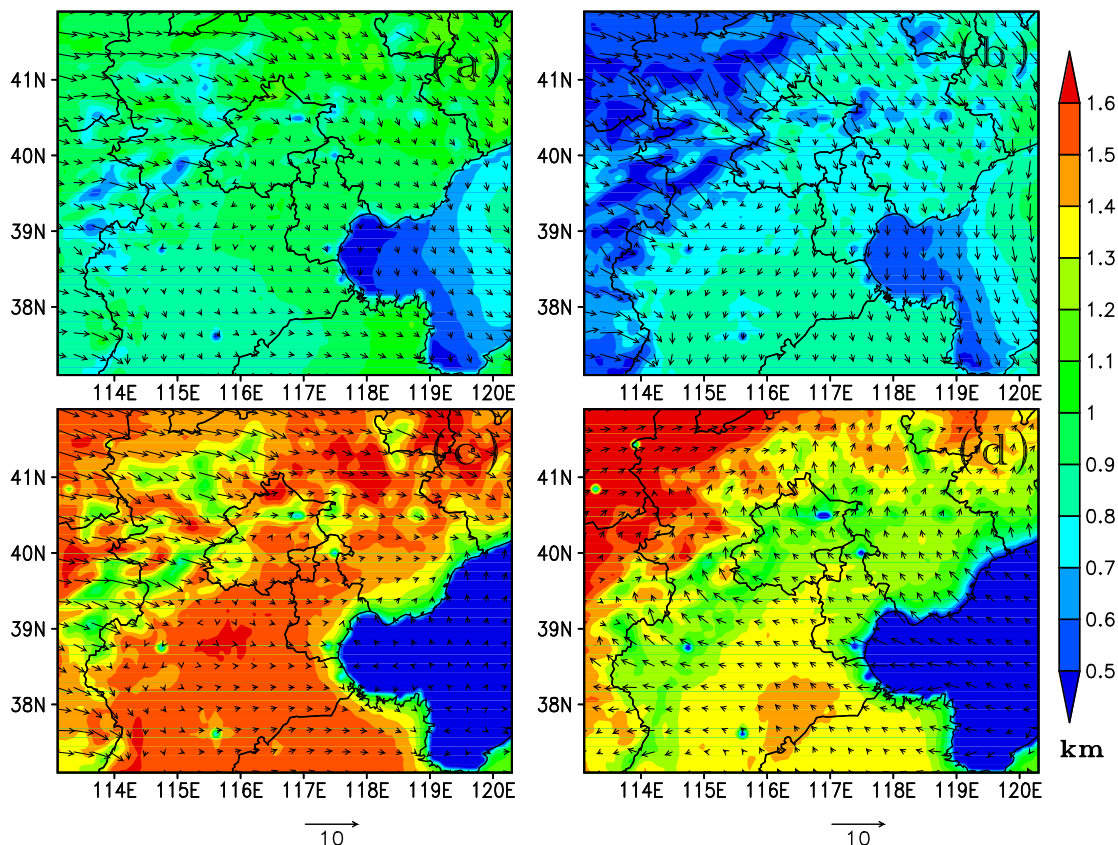
Fig. 3. Averaged planetary boundary layer height and vector winds between 09:00 and 15:00 for autumn (**a**), winter (**b**), spring (**c**), and summer (**d**).

belonged to the fourth group, marked with solid black circles, located in the mountainous area with less dense population and industries.

In order to validate the rationality of the classification, we calculated R and COD pair-wisely and conducted 2 matrices, including 231 results for each statistic. Data abundance, but information indigence. For easy elaborating and understanding, the relative and absolute spatial concentration differences for four categories were separately analyzed using R, CV, and COD based on both the initial FA results and the site geographical characteristics (Table 3). Among the three statistics, R and COD were calculated pair-wisely and then averaged for each group, while CV were computed using all stations in the same group. As shown in Table 3, high R, low CV and COD of O_{3_max} exhibited the homogenous O_3 spatial-temporal variations in the same group and indicated that the classification was reasonable.

As also shown in Table 3, the inter-site correlations for O_{3_max} were the strongest. Correlations ranged between 0.94 and 0.97, with a mean inter-site correlation among all sites of 0.96. O_{3_max} also exhibited the least vari-

ability in absolute levels, with the mean annual CV ranging from 14.5 % to 19.8 %, and the inter-site mean COD of each category was less than 0.20. The statistics of O_3 were similar to that of O_{3_max}. However, all of the statistics were more heterogeneous than that of O_{3_max}, with the mean inter-site correlations ranging between 0.82 and 0.97, the CV ranging between 17.8 % to 37.6 % and the COD ranging between 0.12 to 0.23. NO_x, the primary pollutant, showed mean inter-site correlations for each group that were typically moderate to strong (R range = 0.67–0.93; mean annual inter-site R among all sites = 0.84). As expected, NO_x also exhibited the most variability in absolute levels, with the mean annual CV ranging between 22.1 % and 58.0 % and the inter-site mean COD ranging between 0.17 and 0.36. From the above analysis, two conclusions were made. First, with the high inter-site correlations and the low variability in the absolute levels, O_{3_max} showed great homogeneity among each group, indicating homogenous temporal and spatial variations for the O_{3_max} of each category. Second, compared with the secondary pollutant ozone, NO_x was more heterogeneous, with the lowest correlations and the highest CVs and

Table 3. Inter-site uniformity statistics for four categories.

Site Category	NO$_x$			O$_3$			O$_{3\_max}$		
	R[a]	CV(%)[b]	COD[c]	R	CV(%)	COD	R	CV(%)	COD
Southern plains area	0.93	27.9	0.19	0.96	19.3	0.14	0.97	16.0	0.12
Beijing and its surrounding area	0.87	31.4	0.22	0.97	18.0	0.12	0.97	14.5	0.09
Northwest mountainous area	0.67	58.0	0.36	0.82	37.6	0.23	0.94	19.8	0.13
Eastern coastal area	0.91	22.1	0.17	0.96	17.8	0.13	0.96	13.0	0.09

[a] Correlation coefficients.

[b] Coefficients of variation.

[c] Coefficients of divergence.

CODs. Considering the homogeneity of O$_3$ and O$_{3\_max}$, the heterogeneity of NO$_x$ illustrates the non-linearity between the precursors and ozone production. In other words, the homogeneity of O$_{3\_max}$ among the sites in the different groups probably did not result from the emissions of precursors.

3.3 Temporal variations of O$_3$ and NO$_x$

3.3.1 Seasonal variations

Monthly variations of NO, NO$_2$ and O$_3$ between September 2009 and August 2010 at each site were investigated and the results are shown in Fig. 4. For NO$_x$ at all of the sites, the seasonal variations seem similar, with the highest concentrations appearing in winter and the lowest concentrations appearing in summer. The observed summer valleys of NO$_x$ can be attributed to stronger vertical mixing due to higher PBLH (Fig. 3d), faster transition from NO$_2$ to O$_3$ due to higher temperature and higher wet deposition due to precipitation (Fig. 3). December 2009 was the most polluted month for NO$_x$. In this month, the observed monthly mean mixing ratios of NO and NO$_2$ were 35.5 and 29.1 ppbv, respectively. The observed winter peaks of NO$_x$ can be attributed to weaker vertical mixing due to particularly low PBLH (Fig. 3b), slowest chemical loss due to the lowest temperature (Fig. 2a), solar radiation and oxidant concentrations (Fig. 4), and particularly, much higher anthropogenic emissions from coal-burning in winter.

In contrast with NO$_x$, the secondary pollutant O$_3$ exhibited a reverse seasonal pattern for all of the sites, with the highest mixing ratio appearing in June and the lowest mixing ratio in December. The observed valleys of O$_3$ can be attributed to lower vertical mixing due to lower PBLH (Fig. 3b), stronger titration by NO$_x$ due to higher emissions related to heating and lower photochemical production due to lower temperature (Fig. 2) and solar radiation. Given that July had the highest temperature, higher O$_3$ concentrations were expected in this month. Therefore, the fact that the O$_3$ concentration in June (47.2 ppbv) was much higher than that in July (39.7 ppbv) is of great interest.
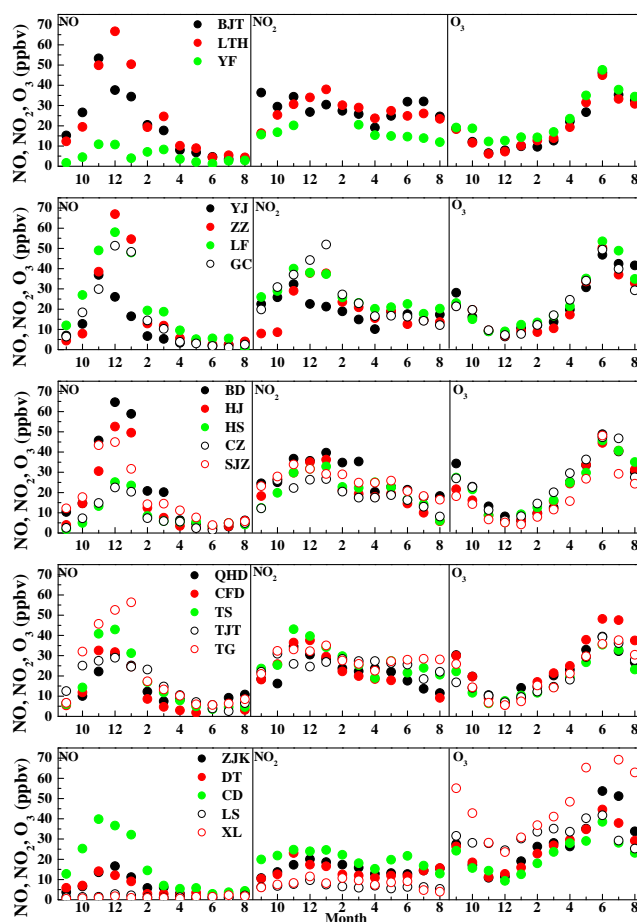

Fig. 4. Seasonal variations of NO$_x$ and O$_3$. The figures are arranged according to the results of site classification. Because the group Beijing and its surrounding areas includes 7 sites and is difficult to present in a figure, this group is divided into 2 subgroups, including Beijing and Beijing's surrounding sites. Therefore, the figures from top to down show sites in Beijing, Beijing's surroundings, southern plains, eastern coastal and northern mountainous areas, respectively.
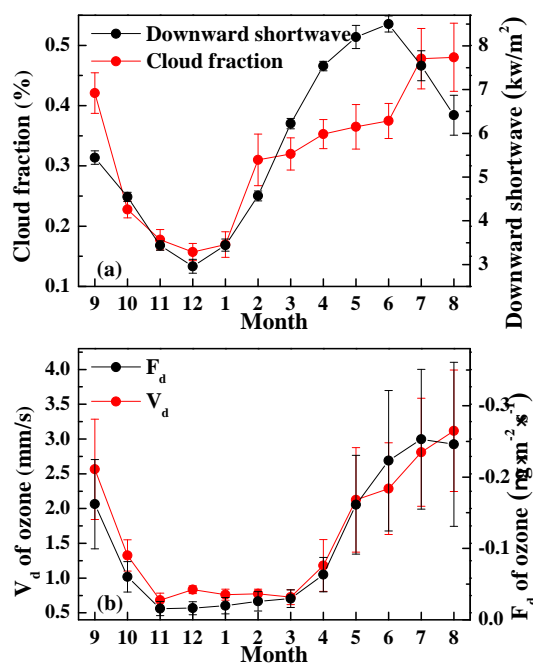
Fig. 5. Simulated monthly variations of cloud fraction and downward shortwave **(a)** and ozone dry deposition velocity and flux **(b)**. The values of cloud fraction and downward shortwave represent averages of simulations taken from 26 weather stations over Northern China. In order to calculate monthly ozone dry deposition flux, the values of ozone dry deposition velocity and flux represent averages of measurements and simulations taken from 22 air quality stations over Northern China.

Ding et al. (2008) suggested two causes of the seasonal peak of O_3 in June over Beijing derived from multi-year records of the MOZAIC aircraft data: more intense crop residue burning in June contributes to emissions of O_3 precursors; and prevailing southerly winds in June facilitate the long-range transport of regional emissions to Beijing. Our observations at 22 sites in summer 2010 presented two interesting cases. One was that all of the sites had similar seasonal patterns, even in the eastern coastal areas. The other interesting case was that although NO_x levels were not significantly different during these two months (20.2 ppbv for July and 21.3 ppbv for June), the O_3 levels still decreased from 47.2 ppbv for June to 39.7 ppbv for July. These results suggest that at least in 2010, this phenomenon could not be attributed to long-range transport due to prevailing southerly winds and changes in local and regional precursor emissions. Wang et al. (2008) suggested another cause of the seasonal peak of O_3 in June at a rural site near Beijing: meteorological influences associated with the summer monsoonal circulation that develops over the North China Plain in July. As shown in Fig. 3, the monthly rainfall for July and August 2010 were 106.8 and 161.4 mm respectively, compared with 47.0 mm for June. As the East Asian summer monsoon

circulation prevailed across the entire eastern part of China, we expected the radiative impact of the monsoonal clouds on ozone to be significant on a regional scale during summer. The results showed that a larger cloud fraction is directly correlated with more precipitation (Fig. 5a). The induced less shortwave radiation because of cloudiness (Fig. 5a) in July then decreased the O_3 photochemical production in Northern China. While we focused on the advantages of meteorology for O_3 photochemical production in June, the process of loss for O_3 should not be ignored. The main processes of loss for O_3 were NO_x titration and dry deposition. Considering the comparable NO_x concentrations in June and July, the differences in NO_x titration could be ignored. In order to quantify the changes of dry deposition flux, we calculated them using the following equation.

$$F_d = -V_d \times C \tag{4}$$

Where F_d is the ozone dry deposition, C is the observed concentrations for ozone and V_d is the ozone dry deposition velocity computed by MCIP based on Wesely method (Wesely, et al., 1989) which is defined as

$$V_d = \frac{1}{R_a + R_b + R_c} \tag{5}$$

Where R_a is the aerodynamic resistance, R_b is the quasi-laminar boundary layer resistance and R_c is the canopy resistance. Among the three resistances, R_c is the highest one for ozone dry deposition velocity (Pan, 2009), so seasonality of V_d is dominated by variation of R_c. Solar radiation and leaf area index (LAI) are two main factors for R_c (Pio et al., 2000). Although solar radiation is highest in June (Fig. 5a), V_d of ozone over crop which dominates the landuse over Northern China is not sensitive to solar radiation (Pan, 2009). Therefore, V_d of ozone is a function of LAI. Considering the highest leaf area index in July and August in Northern hemisphere (van den Hurk, et al., 2003), the highest V_d appeared in August and the lowest value appeared in December (Fig. 5b). The simulated V_d for O_3 in June (2.3 mm s^{-1}) was lower than that in July (2.8 mm s^{-1}) by about 22.9 % over Northern China. In the context, ozone concentrations were highest in June. However, considering the much lower ozone dry deposition velocity compared to July, the dry deposition flux exhibit a 13.5 % decrease from July to June (Fig. 5b). From the above analysis, we arrived at a major conclusion. A decrease in regional O_3 photochemical production was coupled with an increasing O_3 dry deposition in July, and such changes led to the highest O_3 concentrations in June over Northern China. Although some interpretations for the June O_3 peak are given, detailed sources and sinks for surface O_3 over Northern China still need further investigation and additional observational and modeling studies (although beyond the scope of the present analysis) are suggested for further work.
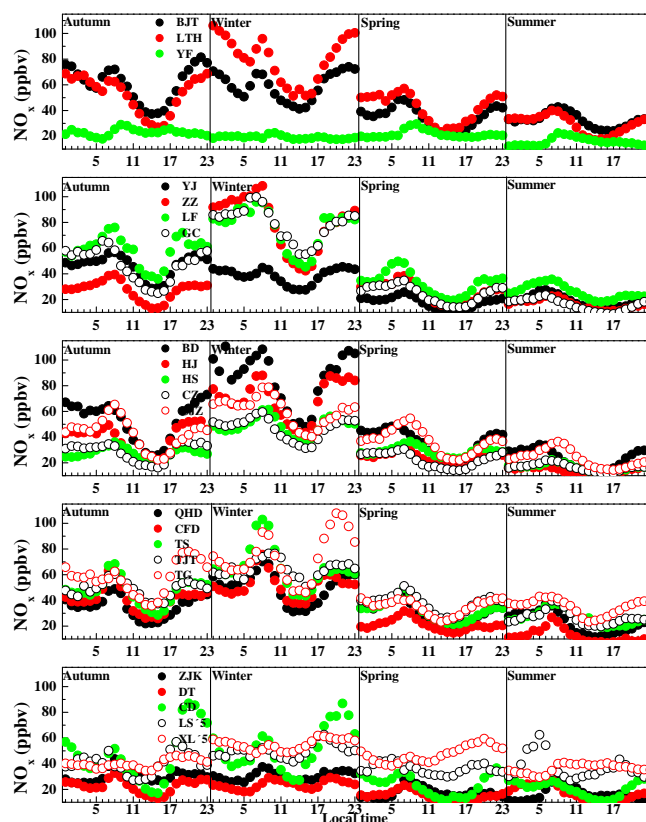
Fig. 6. Diurnal variations of NO_x for four seasons. The figures are arranged according to the results of site classification. Because the group of Beijing and its surrounding areas includes 7 sites and is difficult to present in a figure, this group is divided into 2 subgroups including Beijing and Beijing's surrounding sites. Therefore, the figures from top to down show sites in Beijing, Beijing's surrounding, southern plains, eastern coastal and northern mountainous areas, respectively.
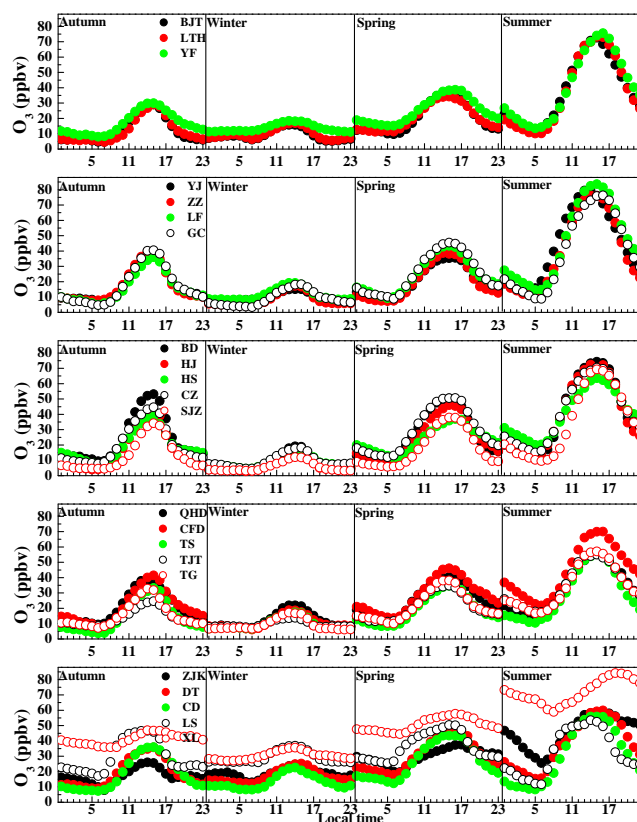
Fig. 7. Diurnal variations of O_3 for four seasons. The figures are arranged according to the results of site classification. Because the group of Beijing and its surrounding areas includes 7 sites and is difficult to present in a figure, this group is divided into 2 subgroups including Beijing and Beijing's surrounding sites. Therefore, the figures from top to down show sites in Beijing, Beijing's surrounding, southern plains, eastern coastal and northern mountainous areas, respectively.

3.3.2 Seasonal average diurnal variations

For each season, the average diurnal variations of NO_x and O_3 mixing ratios were calculated from the hourly average values in the corresponding season. Figure 6 shows the average diurnal variations of the mixing ratios of NO_x in different seasons at the 22 sites. The NO_x mixing ratio shows a diurnal pattern with the maximum appearing in the early morning when the mixing layer is low and stable and the minimum appearing in the afternoon when the photochemical formation and vertical mixing is strong. Figure 6 shows that the mixing ratios of NO_x at night in winter stayed at high levels, which resulted from strong temperature inversion and stable conditions (Fig. 3b) in combination with larger emission from heating in winter. Figure 7 shows the average diurnal variation of the mixing ratios for O_3 in different seasons at the 22 sites. O_3 increased in the early morning after sunrise, reaching a maximum

around 03:00 p.m., and then O_3 decreased in the evening, reaching a minimum around 06:00 a.m., which is immediately before sunrise. Typically, ozone at low-elevation sites peaks in the afternoon, resulting from photochemical formation over the course of the day (Logan, 1989). The diurnal variations of both pollutants were much less significant in winter than in other seasons. The highest average diurnal amplitude for ozone (51.9 ppbv) appeared in summer, and the lowest average diurnal amplitude (11.6 ppbv) appeared in winter. Spring and autumn showed moderate amplitudes of 28.8 ppbv and 28.6 ppbv, respectively. This strong diurnal variation in summer over Northern China is a result of strong photochemical production due to high temperature (Fig. 2a) and high solar radiation (Fig. 5a). Interestingly, the average diurnal variations for NO_x and the ozone concentrations at XL in summer were different from those of other seasons and other sites. The NO_x concentration at XL showed a diurnal pattern with the maximum appearing in

daytime and the minimum appearing at night. Ozone at XL increased in the morning after sunrise, reaching a maximum around 05:00 p.m. and then decreased at night, reaching a minimum around 08:00 a.m. Both the peak and valley hours were delayed by about 2 hours compared with other sites. The high mixing ratios of ozone occurred at 05:00 p.m., combined with the daytime peak in NO_x mixing ratios (Fig. 6), indicating the arrival of more polluted air, consistent with the change in mean flow pattern in summer (Fig. 3d). In addition, the diurnal variations of ozone were much less significant at XL than those at other sites. Considering the delayed ozone peak and mean flow pattern in summer, the weak diurnal variation of ozone indicated the main source of ozone at XL may be transport. Consistent with our hypothesis, previous observations at other surface sites near northerly mountainous areas over Northern China showed similar diurnal cycles in summer (Wang et al., 2008; Lin et al., 2008).

3.3.3 Exceedances of O_3

The Chinese Ambient Air Quality Standards (CAAQS, revised GB 3095–1996 of Chinese National Air Quality standards) are classified into three grades aiming at natural scenic spots, residential areas and industrial areas, respectively. The thresholds of each grade are shown in Table S2. The value of the WHO interim target-1 (IT-1) for daily maximum 8-h mean (82 ppbv), an intermediate target for populations with O_3 concentrations above this level, was proposed as one of the indexes for the protection of human health effects (WHO, 2006). On account of human health, exceedances of O_3 were computed using CAAQS Grade II (102 ppbv) and WHO IT-1 standards, respectively. The hourly O_3 mixing ratio exceeding Grade II occurred mainly between May and September. During the observation period, the average exceedances at the 22 sites of the daily maximum O_3 when the O_3 level exceeded Grade II were found to be 0.7 %, 0.0 %, 1.9 %, and 18.2 % in autumn, winter, spring and summer, respectively. 8-h mixing ratio was also calculated for the O_3 at the 22 sites and found to be 1.4 %, 0.0 %, 2.8 % and 26.2 % in autumn, winter, spring and summer, respectively. Therefore, the daily maximum 1-h and 8-h mean exceedances of CAAQS and IT-1 mainly occurred in summer, with the largest appearing in June. According to these statistics, O_3, which threatens human health, is one of the main pollutants over Northern China in summer. In the following sections, we will focus on the spatial distribution for summer O_3, and then give some interpretations for summer O_3 spatial distribution over Northern China. Finally, combined with the smog production algorithm and space-based $HCHO/NO_2$ column ratio, detailed control strategies for summer O_3 can be suggested and evaluated for different areas over Northern China.
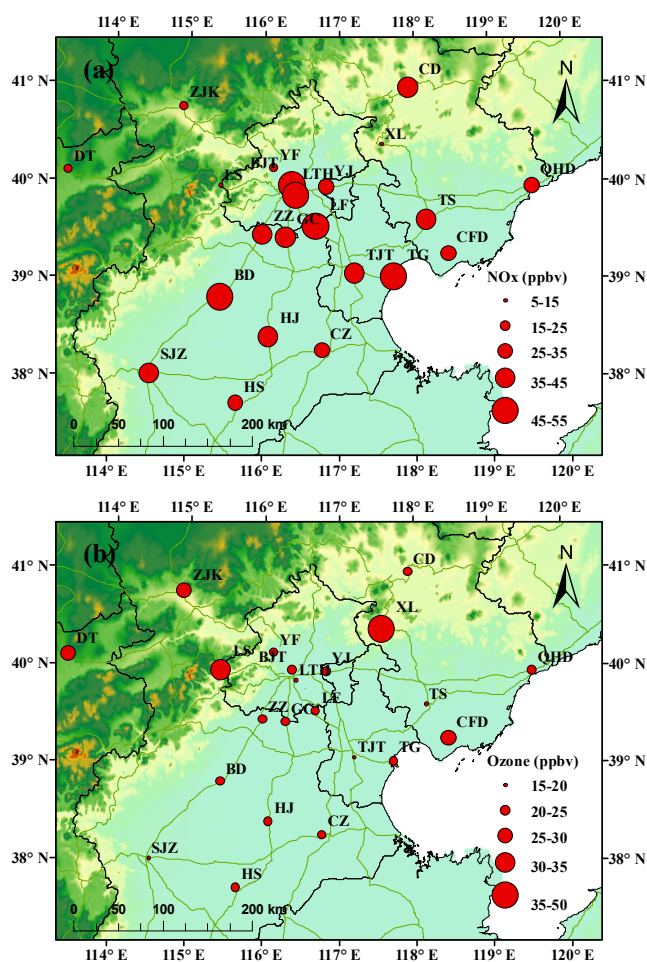

Fig. 8. Spatial distribution of average NO_x **(a)** and O_3 **(b)** over Northern China.

3.4 Spatial variations of O_3 and NO_x

3.4.1 Seasonal average spatial variations of O_3 and NO_x

Spatial distributions of surface NO_x and O_3 for the annual mean are presented in Fig. 8a and b. Similar patterns were found for different seasons in Figs. S2 and S3 for NO_x and O_3, respectively. The annual mean NO_x mixing ratios were relatively high over the plains, but low over the mountainous areas. The lowest NO_x concentrations were found in two rural sites over mountainous areas at LS (8.2 ppbv) and XL (9.1 ppbv), as expected. The average of the other three mountainous sites was 28.5 ppbv, which was also much lower than the average concentration over the plains areas (39.8 ppbv). The highest annual mean NO_x concentration (55.4 ppbv) appeared in BJT. In TG, the average annual mean NO_x concentration was 49.7 ppbv, second only to that in BJT. This spatial distribution of NO_x over Northern China did not match well with NO_x emissions, especially over the red-square areas
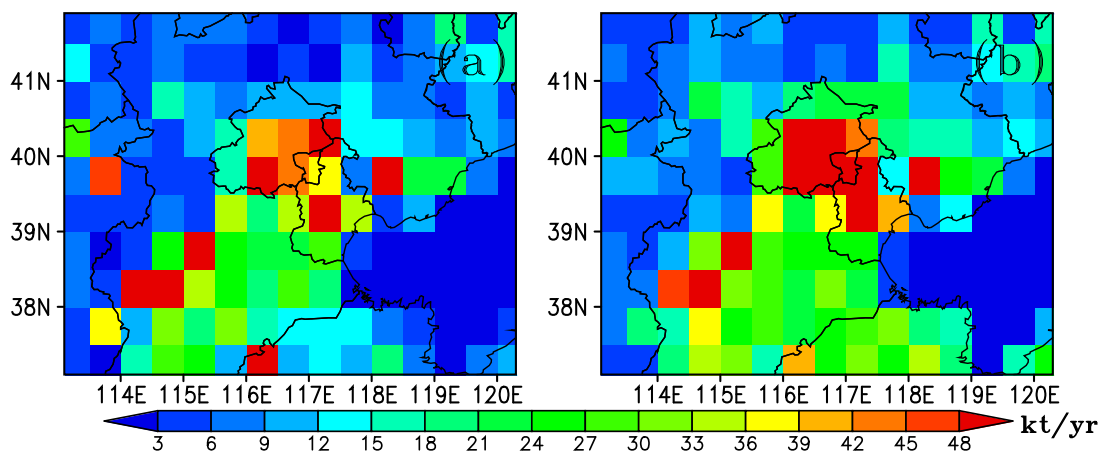
Fig. 9. NO_x **(a)** and VOCs **(b)** emissions in 2006.

Table 4. Spatial statistics of meteorological parameters for four categories.

Site Category	T^a	RH^b	CF^c	SW^d
	°C	%	%	$W\,m^{-2}$
Southern plains area	30.5	50.0	40.9	780.5
Beijing and its surrounding area	29.8	49.7	34.7	809.4
Northwest mountainous area	26.0	49.4	32.0	813.3
Eastern coastal area	28.2	59.0	39.5	780.3

[a] Temperature.

[b] Relative humidity.

[c] Cloud fraction.

[d] Downward shortwave.

(Fig. 9a). The total NO_x emissions (as NO_2) in Beijing, Tianjin and Hebei are 2.0 Tg in 2006 and accounted for 42.0 % from power plants, 23.1 % from automobiles, 29.0 % from industry and 5.9 % from residential sources (Zhang et al., 2009). Considering the higher stacks of power plants and industry, Hao et al. (2000) indicated that automobile sources contributed 67 % to the NO_x concentration, which implies that vehicle emissions are the most important air pollutant source in Beijing. This phenomenon was also the main reason for the mismatch between emissions and ambient concentrations.

In contrast to NO_x, the annual mean O_3 concentrations are relatively high over the northwestern mountainous areas but low over the plains. The annual mean O_3 mixing ratio at DT, LS, XL and ZJK were 25.8, 31.8, 49.3 and 28.37 ppbv, respectively, with an average of 33.6 ppbv. However, the average annual O_3 mixing ratio for each site over the North China Plain was lower than 25.0 ppbv, with an average of 21.9 ppbv. Therefore, the high NO_x emissions over the plains, especially in the urban areas, scavenge O_3 from the air in the plains, thus decreasing the O_3 levels in these areas.

3.4.2 Spatial variations and interpretations of summer maximum O_3

Spatial distributions of exceedances for average daily 1-h maximum ozone in summer are presented in Fig. 10a. Similar patterns were found for the exceedances of average daily 8-h maximum ozone in Fig. S4. Different from the spatial distribution of ozone annual mean, the spatial distributions of the exceedances for daily 1-h and 8-h maximum ozone in summer were consistent with the classification of the regional sites, with the highest values over Beijing and the surrounding areas and the lowest values over the northwestern mountainous area. The exceedances of daily 1-h maximum ozone at DT, CD, LS and ZJK in the mountainous area were 3.3, 3.3, 5.5 and 11.1 %, respectively, with the average being 5.8 %. However, the highest exceedances of daily 1-h and 8-h maximum ozone appeared at XL (45.3 % for 1-h and 70.9 % for 8-h maximum ozone) in the mountainous area, which are downwind of Beijing, Tianjin and Hebei, showing the strong influence of upwind areas. At CFD, QHD, TG, TJT and TS in the eastern coastal areas, exceedances of daily 1-h maximum ozone were 15.2, 3.3, 4.9, 8.0 and 5.8 %, with the average of 6.1 %, the second lowest only to the one in the mountainous areas. The relative highest exceedances of daily 1-h maximum ozone appeared over Beijing and the surrounding areas with the average of 31.3 %. Over the southern plains moderate exceedance of daily 1-h maximum ozone was presented with an average of 15.7 %. According to the above analysis, we found that the average daily maximum ozone concentrations for summer were distinct over different areas. Therefore, what are the sources in different areas? Kley et al. (1999) indicated O_x, defined as: $O_x = O_3 + NO_2$, a quasi-conservative quantity, where the concentration of O_x represented the photochemical production of ozone. Figure 13 shows the spatial distribution of the
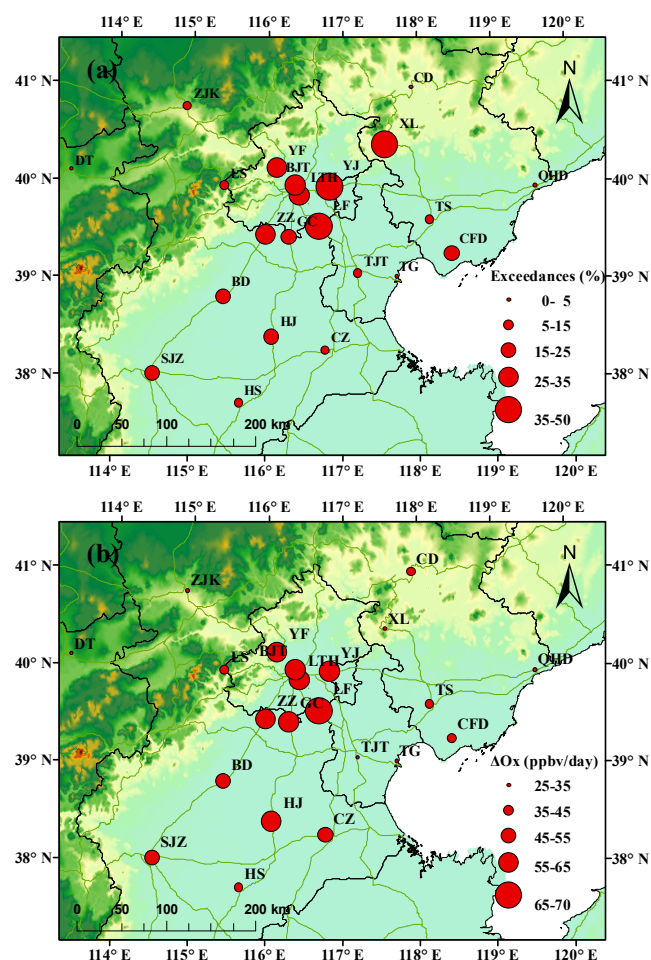
Fig. 10. Spatial distribution of exceedances for average daily 1-h maximum O₃ **(a)** and averaged daily O$_x$ range **(b)** for summer.

average daily O$_x$ range for summer. As shown in Fig. 10b, the spatial distribution of the average daily O$_x$ ranges in summer were similar to the spatial distribution of exceedances for daily 1-h maximum ozone except at XL. XL, a regional site influenced by transport, exhibited the lowest O$_x$ production rate (25.3 ppbv d^{-1}), as expected. The average photochemical production rate of four other mountainous sites and the eastern coastal sites were 35.9 ppbv d^{-1} and 35.9 ppbv d^{-1}, respectively, which were also much lower than that over the southern plains (48.8 ppbv d^{-1}) and Beijing and its surrounding areas (61.2 ppbv d^{-1}). These results exhibit the strongest ozone photochemical productions in plains, especially over Beijing and its surrounding area.

Soloman et al. (2000) indicated that among the four factors, meteorology, atmospheric chemistry, emissions and deposition, which lead to the accumulation of O₃ in the troposphere, meteorological processes are dominant, causing large day-to-night, day-to-day, season-to-season, and year-to-year

variations. High concentrations of O₃ observed during stagnant conditions are characterized by high ambient temperatures, low wind speeds, ample sunlight, and the presence of abundant local or regional emissions of precursor species. Meteorological conditions are found to be the main driving force for temporal variability. Yet, there is the unanswered question, what controls spatial variability in O₃? Do meteorological processes also control O₃ spatial variations and O₃ production in these four different areas over Northern China? Figure 11 shows the simulated average temperature, relative humidity, downward shortwave, and cloud fraction between 09:00 and 15:00 for summer. In order to elaborate the spatial differences of the meteorological conditions, simulated results in WRF were extracted and used to compute the mean levels of temperature, relative humidity, downward shortwave and cloud fraction for each area (Table 4). As shown in Table 4, Figs. 3d and 11, four different areas show different meteorology. Meteorology simulated over Beijing and its surrounding areas is characterized by high temperatures, high downward shortwave, low cloud cover, low relative humidity, weak southeast winds and relatively low PBLH compared with the southern plains. Similar to Beijing and its surrounding areas, the southern plains have a meteorology that is characterized by high temperatures, low relative humidity and weak southeast winds, but relatively low downward shortwave, high PBLH and high cloud cover. However, the meteorology of the eastern coastal area is characterized by low temperatures, low downward shortwave, high cloud cover, high relative humidity, low PBLH and strong southeast winds. In addition, meteorology over the northwestern mountainous area shows another feature, which is characterized by the lowest temperature, lowest relative humidity, highest downward shortwave, strong west winds and high PBLH.

From the above analysis, we found that the meteorology over Beijing and its surrounding areas and the northwestern mountainous area is the most and the least fit for O₃ photochemical production, respectively. In addition, O₃ showed a clear increasing trend from the eastern coastal area to the mountain front area. The trend of increasing ozone along the direction of the prevailing wind was consistent with the widespread regional-scale transport of oxidants. These results, consistent with the spatial variations of O₃ concentrations and O$_x$ production rates, illustrated that the spatial distribution of summer O₃ was dominated by the meteorology of different areas over Northern China. However, what are the roles of emissions over Northern China? As shown in Fig. 9 (Zhang et al., 2009), the plains area corresponded to more industrialization and automobiles, and the NO$_x$ and VOCs emissions for most of the grid (0.5 degree × 0.5 degree) over the plains were both over 18 kt yr^{-1}. However, in the mountainous areas, NO$_x$ and VOCs were both less than 6 kt yr^{-1} for most of the grid. The emissions of precursors were weakly correlated with O₃ concentrations over Northern China, especially in the eastern
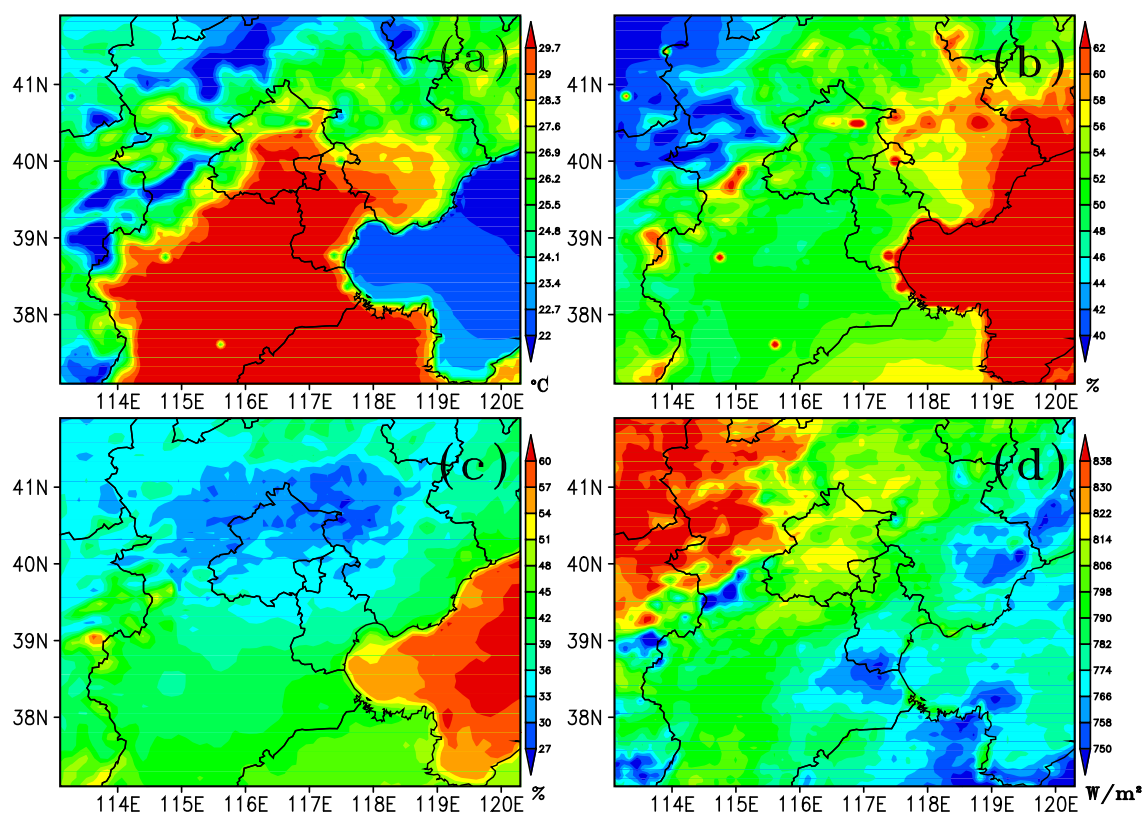
Fig. 11. Simulated average temperature **(a)**, relative humidity **(b)**, cloud fraction **(c)**, and downward shortwave **(d)** between 09:00 and 15:00 for summer.

coastal area, which exhibited high emissions of precursors but low O_3 concentrations and O_x production rates. Although there is no direct relationship between the emissions of precursors and O_3 concentrations, it should be noted that abundant emissions over the plains are essential conditions for O_3 photochemical production over Beijing and its surrounding area. From the results presented above, two major conclusions can be drawn. First, the O_3 photochemical production efficiency was highly non-linear and abundant NO_x and VOCs emissions over the eastern coastal area could not result in high O_3 concentrations in this area, indicating that the observed daily maximum O_3 concentrations were dominated by meteorological processes. Second, the abundant NO_x and VOCs emissions were essential for ozone production. Therefore, the domination of the meteorological process was based on the present spatial distribution of emissions. Considering the similar year-to-year meteorology in summer, the reduction of emissions of precursors would be a unique and effective method to change the spatial variations of summer O_3 and decrease the regional photochemical pollution over Northern China.

3.5 O_3-NO_x-VOCs sensitivity diagnosis and possible implications for future air quality control strategies in Northern China

In order to diagnose the O_3-NO_x-VOCs sensitivity, the $E(t)$ and HCHO/NO_2 column ratio were computed using ground and satellite observations, respectively. Figure 12 shows the spatial distribution of the extent of reaction over Northern China between June and August 2010. The $E(t)$s of nearly all of the sites except XL were less than 0.4, which indicated NO_x-saturated conditions at these sites. As discussed above, the main source of ozone for XL is the transport from upwind areas. Photochemical production in XL was lower than that at other sites, as shown by the much higher $E(t)$ value (0.74) at XL. This high value of $E(t)$ illustrates that the O_3-NO_x-VOCs sensitivity of XL should generally be considered transitional or indeterminate. Figure 13 shows the GOME-2 HCHO/NO_2 column ratio over Northern China between June and August 2010. The resulting gradients of NO_x-saturated conditions during summer over the North China Plain but NO_x-sensitive conditions over the northern mountainous areas, were consistent with the results from the SP algorithm and photochemical model calculations of Tang et

al. (2010b). However, GOME HCHO/NO$_2$ ratios greater than one during summer over eastern China indicated NO$_x$-sensitive conditions in 1997 (Martin, et al., 2004), which is inconsistent with our analysis.

Since 1997, with the strong economic and industrial development in China, the anthropogenic VOCs and NO$_x$ emissions have significantly changed. Smedt et al. (2010) showed that the HCHO trend in the BTH area was $4 \pm 1.4 \%$ yr^{-1} between 1997 and 2009, while the NO$_2$ trend in Beijing is $11 \pm 4 \%$ yr^{-1} between 1996 and 2006 (van der A et al., 2006, 2008). Calculated using the above HCHO and NO$_2$ trends, the HCHO column concentrations increased 1.7 times from 1997 to 2010, while the NO$_2$ column concentrations increased 3.9 times in the same period. In other words, the growth rate of NO$_2$ was much higher than that of HCHO, indicating a decreasing trend of HCHO/NO$_2$ between 1997 and 2010, which induced a clear transition from NO$_x$ sensitivity in 1997 to NO$_x$ saturation in 2010 over the plains.

The above finding is extremely important to the design of an effective O$_3$ control strategy for Northern China. Our results suggest that the control of VOCs would be most effective for controlling the ozone over North China Plain, while NO$_x$ control would be counterproductive in this area. In addition, NO$_x$ control would be the most effective measure for controlling ozone over the mountainous areas, related to the lower emissions in this area. In this context, as noted earlier, the concentrations of O$_3$ in the upwind region are low. However, the high VOCs and NO$_x$ emissions in this area (Figs. 6 and 9) contribute significantly to the O$_3$ precursors in the downwind regions. Therefore, an effective O$_3$ control strategy also needs to consider O$_3$ formation from the reaction of its precursors during the transport from the upwind region.

4 Conclusions

As one of the developing urban agglomerations in China, the BTH area has been confronted with severe air pollution for several decades. The air pollutants originate from sources both in the urban areas and in the countryside, particularly in the polluted North China Plain. To make effective policies for controlling the photochemical pollution over Northern China, it is crucial to know the air quality in this area. During the Project of Atmospheric Combined Pollution Monitoring over Beijing and its surrounding areas, 22 sites over Northern China were selected as representative sites. The major field campaign conducted in 2009–2010 allowed the observation of the concentrations and spatial-temporal variations of ozone and nitrogen oxide over Northern China for the first time.

During the observation period, we examined the seasonal, diurnal and spatial variations of meteorological factors ozone and NO$_x$ over northern China. Our results suggest distinct seasonal and diurnal cycles in meteorology, ground-
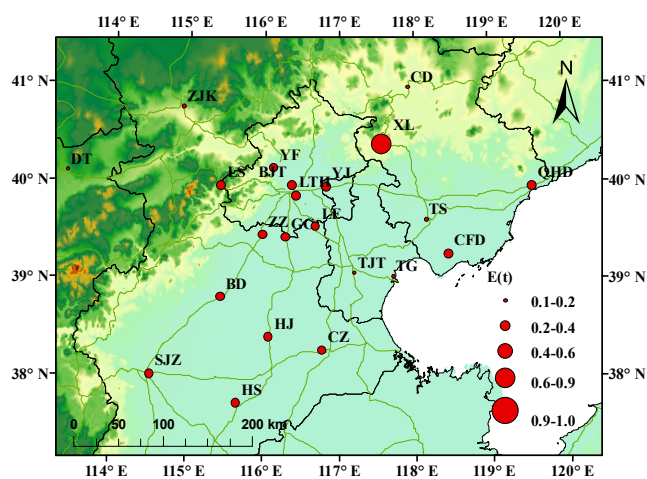

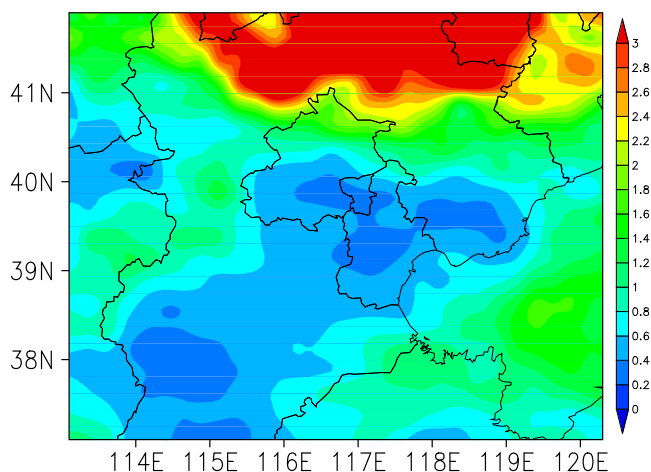**Fig. 12.** Spatial distribution of $E(t)$ over Northern China in summer.

Fig. 13. HCHO/NO$_2$ ratio of GOME-2 for summer.

level ozone, and NO$_x$ over Northern China. Lower ozone concentrations were generally observed in winter and during early morning hours, while high ozone levels were typically found in summer and in the afternoon. The annual average ozone concentrations were lower in plains areas compared with the sites in the northwestern mountainous areas. The lower ozone concentrations in the plains were due to the titration effect of high NO$_x$ emission in this area. When the summer ozone was separately analyzed with the meteorological model, the emissions, the smog production algorithm and space-based observations, four major conclusions were derived:

1. A decrease in regional O_3 photochemical production seems to be coupled with increasing ozone dry deposition in July, and this combination leads to the highest ozone concentrations in June over Northern China.

2. The 22 sites can be aggregated into four categories based on daily 1-h maximum ozone: the eastern coastal area, southern plains area, Beijing and the surrounding area, and the northwestern mountainous area. These results indicate different ozone maximum concentrations over different areas, with the highest and lowest frequency of exceedances of national air quality thresholds in Beijing and its surrounding area and the northwestern mountainous area, respectively.

3. Spatial variations in the daily maximum ozone are dominated by meteorological processes over Northern China. The highest daily maximum ozone concentrations observed over Beijing and the surrounding area are found to be mainly dominated by high temperatures, high downward shortwave, low cloud cover, low relative humidity, weak southeast winds and low PBLH, with the presence of abundant NO_x and VOCs emissions over the plains.

4. The $E(t)$ and $HCHO/NO_2$ ratio suggest that O_3 photochemistry was usually in the VOCs-limited regime over the plains in summer. Our results suggest that control of VOCs would be most effective for controlling the ozone over the North China Plain, while NO_x control would be counterproductive in this area. However, considering the high emissions in the upwind area, an effective O_3 control strategy will also need to consider the O_3 formation from reactions by its precursors during the transport from the upwind region.

Supplementary material related to this article is available online at: http://www.atmos-chem-phys.net/12/2757/2012/ acp-12-2757-2012-supplement.pdf.

References

Akimoto, H.: Global air quality and pollution, Science, 302, 1716–1719, 2003.

Blanchard, C. L., Lurmann, F. W., Roth, P. M., Jeffries, H. E., and Korc, M.: The use of ambient data to corroborate analyses of ozone control strategies, Atmos. Environ., 33, 369–381, 1999.

Blanchard, C. L.: Ozone process insights from field experiments–Part III: extent of reaction and ozone formation, Atmos. Environ., 34, 2035–2043, 2000.

Blanchard, C. L. and Stoeckenius, T.: Ozone response to precursor controls: comparison of data analysis methods with the predictions of photochemical air quality simulation models, Atmos. Environ., 35, 1203–1215, 2001a.

Blanchard, C. L. and Fairley, D.: Spatial mapping of VOC and NO_x-limitation of ozone formation in central California, Atmos. Environ., 35, 3861–3873, 2001b.

Boersma, K. F., Eskes, H. J., and Brinksma, E. J.: Error Analysis for Tropospheric NO_2 Retrieval from Space, J. Geophys. Res., 109, D04311, doi:10.1029/2003JD003962, 2004.

Bromwich, D. H., Bai, L., and Bjarnason, G. G.: High-resolution regional climate simulations over Iceland using Polar MM5, Mon. Weather Rev., 133, 3527–3547, 2005.

Bronnimann, S., Buchmann, B., and Wanner, H.: Trends in near-surface ozone concentration in Switzerland: the 1990s, Atmos. Environ., 36, 2841–2852, 2002.

Byun, D. W. and Ching, J. K. S.: Science Algorithms of the EPA Models-3 Community Multiscale Air Quality (CMAQ) Modeling System, Office of Research and Development, Washington, DC 20460, EPA/600/R-99/030, 1999.

Chai, F. H., Xue, Z. G., Du, S. Y., Ling, X., and Guo, J. L.: Effects of air pollution control measures in Beijing, Environ. Protect., 7, 49–52, 2006 (in Chinese).

Chan, C. K. and Yao, X.: Air pollution in mega cities in China, Atmos. Environ., 42, 1–42, 2008.

Cheng, S., Chen, D., Li, J., Guo, X. R., and Wang, H. Y.: An ARPS-CMAQ modeling approach for assessing the atmospheric assimilative capacity of the Beijing metropolitan region, Water Air Soil. Pollut., 181, 211–224, 2007.

Cyrys, J., Pitz, M., Heinrich, J., Wichmann, H.-E., and Peters, A.: Spatial and temporal variation of particle number concentration in Augsburg, Germany, Sci. Total Environ., 401, 168–175, 2008.

Dahlbeck, A. and Stamnes, K.: A new spherical model for computing the radiation field available for photolysis and heating at twilight, Planet. Space Sci., 39, 671–683, 1991.

Duncan, B. N., Yoshida, Y., and Olson J. R.: Application of OMI observations to a space-based indicator of NO_x and VOC controls on surface ozone formation, Atmos. Environ., 44, 2213–2223, 2010.

Ding, G. A., Chen, Z. Y., Gao, Z. Q., Yao, W. Q., Li, Y., Cheng, X. H., Meng, Z. Y., Yu, H. Q., Wong, K. H., Wang, S. F., and Miao, Q. J.: Vertical structures of PM_{10} and $PM_{2.5}$ and their dynamical character in low atmosphere in Beijing urban areas, Sci. China Ser. D-Earth Sci., 35, 31–44, 2005.

Emery, C. A., Tai, E., and Yarwood, G.: Enhanced meteorological modeling and performance evaluation for two Texas ozone episodes, Project Report prepared for the Texas Natural Resource Conservation Commissions, ENVIRON International Corporation, Novato, CA, 2001.

Hanna, S. R. and Yang, R. X.: Evaluations of mesoscale models'

simulations of near-surface winds, temperature gradients, and mixing depths, J. Appl. Meteorol., 40, 1095–1104, 2001.

Hao, J. M., He, D. Q., Wu, Y., Fu, L., and He, K. B.: A study of the emission and concentration distribution of vehicular pollutants in the urban area of Beijing. Atmos. Environ., 34, 453–465, 2000.

Hao, J. M., Wang, L. T., Li, L., Hu, J. N., and Yu, X. C.: Air pollutants contribution and control strategies of energy-use related sources in Beijing, Sci. China Ser. D-Earth Sci., 35(Suppl I), 115–122, 2005.

Hines, K. M. and Bromwich, D. H.: Development and Testing of Polar Weather Research and Forecasting (WRF) Model. Part I: Greenland Ice Sheet Meteorology, Mon. Weather Rev., 136, 1971–1989, 2008.

Houghton, J. T., Ding, Y., Griggs, D. J., Noguer, M., van der Linden, P. J., Dai, X., Maskell, K., Johnson, C. A.: Intergovernmental panel on Climate Change(IPCC), Climate Change 2001: The science of Climate Change, Cambridge Univ. Press, New York, USA, 881 pp., 2001.

Huang, C., Chen, C. H., Li, L., Cheng, Z., Wang, H. L., Huang, H. Y., Streets, D. G., Wang, Y. J., Zhang, G. F., and Chen, Y. R.: Emission inventory of anthropogenic air pollutants and VOC species in the Yangtze River Delta region, China, Atmos. Chem. Phys., 11, 4105–4120, doi:10.5194/acp-11-4105-2011, 2011.

Jacob, D. J., Logan, J. A., and Murti, P. P.: Effect of rising Asian emissions on surface ozone in the United States, Geophys. Res. Lett., 26, 2175–2178, 1999.

Johnson, G. M.: A simple model for predicting the ozone concentration of ambient air. Proceedings of the Eighth International Clean Air Conference, Melbourne, Australia, 715–731, 1984.

Johnson, G. M. and Quigley, S. M.: A universal monitor for photochemical smog, Air & Waste Management Association 82nd Annual Meeting and Exhibition, Anaheim, California, Paper 89–29.8, 1989.

Jonson, J. E., Simpson, D., Fagerli, H., and Solberg, S.: Can we explain the trends in European ozone levels?, Atmos. Chem. Phys., 6, 51–66, doi:10.5194/acp-6-51-2006, 2006.

Kely, D., Kleinmann, M., Sanderman, H., and Krupa, S.: Photochemical oxidants: state of the science, Environ. Pollut., 100, 19–42, 1999.

Lee, S. H., Akimoto, H., Nakane, H., Kurnosenko, S., and Kinjo, Y.: Lower tropospheric ozone trend observed in 1989-1997 at Okinawa, Japan, Geophys. Res. Lett., 25, 1637–1640.1998.

Lelieveld, J., van Aardenne, J., Fischer, H., de Reus, M., Williams, J., and Winkler, P.: Increasing ozone over the Atlantic Ocean, Science, 304, 1483–1487, 2004.

Li, L., Chen, C. H., Fu, J. S., Huang, C., Streets, D. G., Huang, H. Y., Zhang, G. F., Wang, Y. J., Jang, C. J., Wang, H. L., Chen, Y. R., and Fu, J. M.: Air quality and emissions in the Yangtze River Delta, China, Atmos. Chem. Phys., 11, 1621–1639, doi:10.5194/acp-11-1621-2011, 2011.

Lin, C.-Y. C., Munger, J. W., Fiore, A. M., and Jacob, D. J.: Increasing background ozone in surface air over the United States, Geophys. Res. Lett., 27, 3465–3468, 2000.

Lin, W., Xu, X., Zhang, X., and Tang, J.: Contributions of pollutants from North China Plain to surface ozone at the Shangdianzi GAW Station, Atmos. Chem. Phys., 8, 5889–5898, doi:10.5194/acp-8-5889-2008, 2008.

Liu, S. C.: Possible effects on tropospheric O_3 and OH due to NO emissions, Geophys. Res. Lett., 4, 325–328, 1977.

Logan, J. A.: Ozone in rural areas of the United States, J. Geophys. Res., 94, 8511–8532, 1989.

Lu, Z., Streets, D. G., Zhang, Q., Wang, S., Carmichael, G. R., Cheng, Y. F., Wei, C., Chin, M., Diehl, T., and Tan, Q.: Sulfur dioxide emissions in China and sulfur trends in East Asia since 2000, Atmos. Chem. Phys., 10, 6311–6331, doi:10.5194/acp-10-6311-2010, 2010.

Kim, E., Hopke, P. K.., Pinto, J. P., and Wilson, W. E.: Spatial variablity of fine particle mass, components, and source contributions during the regional air pollution study in St. Louis, Environ. Sci. Technol., 39, 4172–4179, 2005.

Krudysz, M. A., Froines, J. R., Fine, P. M., and Sioutas, C.: Intracommunity spatial variation of size-fractionated PM mass, OC, EC, and trace elements in the Long Beach, CA area, Atmos. Environ., 42, 5374–5389, 2008.

Martin, R. V., Fiore, A. M., and Donkelaar, A. V.: Spase-based diagnosis of surface ozone sensitivity to anthropogenic emissions, Gerophys. Res. Lett., 31, L06120, doi:10.1029/2004GL01941, 2004.

Meng, Z. Y., Xu, X. B., Yan, P., Ding, G. A., Tang, J., Lin, W. L., Xu, X. D., and Wang, S. F.: Characteristics of trace gaseous pollutants at a regional background station in Northern China, Atmos. Chem. Phys., 9, 927–936, doi:10.5194/acp-9-927-2009, 2009.

National Bureau of Statistics of China: China Statistical Yearbook 2010, http://www.stats.gov.cn/tjsj/ndsj/2010/indexch.htm, last access: 16 January 2012, China Statistics Press, 2010.

National Research Council (NRC): Committee on tropospheric ozone formation and measurement, Rethinking the ozone problem in urban and regional air pollution, National Academy Press, 1991.

Oltmans, S. J., Lefohn, A. S., Scheel, H. E., Harris, J. M., Levy II, H., Galbally, I. E., Brunke, E.-G., Meyer, C. P., Lathrop, J. A., Johnson, B. J., Shadwick, D. S., Cuevas, E., Schmidlin, F. J., Tarasick, D. W., Claude, H., Kerr, J. B., Uchino, O., and Mohnen, V.: Trends of ozone in the troposphere, Geophys. Res. Lett., 25, 139–142, 1998.

Palmer, P. I., Jacob, D. J., Chance, K., Martin, R. V., Spurr, R. J. D., Kurosu, T. P., Bey, I., Yantosca, R., Fiore, A., and Li, Q. B.: Air mass factor formulation for spectroscopic measurements from satellites: Application to formaldehyde retrievals from the Global Ozone Monitoring Experiment, J. Geophys. Res., 106, 14539–14550, 2001.

Pan, X.: Observation and modeling studies on the dry deposition of major air pollutants in North China, Ph.D thesis, Chinese Academy of Sciences, 157 pp., 2009.

Parrish, D. D., Dunlea, E. J., Atlas, E. L., Schauffler, S., Donnelly, S., Stroud, V., Goldstein, A., Millet, D., McKay, M., Jaffe, D., Price, H., Hess, P., Flocke, F., and Roberts, J. M.: Changes in the photochemical environment of the temperate North Pacific troposphere in response to increased Asian emissions, J. Geophys. Res., 109, D23S18, doi:10.1029/2004JD004978, 2004.

Pinto, J. P., Lefohn, A. S., and Shadwick, D. S.: Spatial variability of $PM_{2.5}$ in urban areas in the United States, J. Air Waste Manage. Assoc., 54, 440–449, 2004.

Pio, C. A., Feliciano, M. S., Vermeulen, A. T., and Sousa, E. C.: Seasonal variability of ozone dry depostion under southern European climate conditions, in Portugal, Atmos. Environ., 34, 195–205, 2000.

POPG: Ozone in the United Kingdom, Fourth Report of the UK photochemical oxidants review group, Department of the Environment, Transport and the Regions, London, UK, 1997.

Sarnat, J. A., Moise, T., Shpund, J., Liu, Y., Pachon, J. E., Qasrawi, R., Abdeen, Z., Brenner, S., Nassar, K., Saleh, R., and Schauer J. J.: Assessing the spatial and temporal variability of fine particulate matter components in Israeli, Jordanian, and Palestinian cities, Atmos. Environ., 44, 2383–2392, 2010.

Seinfeld, J. H. and Pandis, S. N.: Atmospheric Chemistry and physics, From Air Pollution to Climate Changes, Wiley, New York, USA, 1326 pp., 1998.

Shao, M., Zhang, Y. H. Zeng, L. M., Tang, X. Y., Zhang, J., Zhong, L. J., and Wang, B. G.: Ground-level ozone in the Pearl River Delta and the roles of VOC and NO_x in its production, J. Envrion. Manage., 90, 512–518, 2009.

Skamarock, W. C., Klemp, J. B., Dudhia, J., Gill, D. O., Barker, M., Duda, K. G., Huang, X.-Y., Wang, W., and Powers J. G.: A description of the Advanced Research WRF Version 3, NCAR/TN–475+STR, 2008.

Smedt, I. D., Stavrakou, J., Müller, J.-F., Hao, N., Valks, P., Loyola, D., and Roozendael, M. V.: H_2CO columns retrieved from GOME-2: First scientific results and progress towards the development of an operational product, proceedings of the EUTMETSAT conference, 2009.

Smedt, I. D., Stavrakou, T., Müller, J.-F., van der A, R. J., and Roozendael, M. V.: Trend detection in satellite observations of formaldehyde tropospheric columns, Geophys. Res. Lett., 37, L18808, doi:10.1029/2010GL044245, 2010.

Solomon, P., Cowling, E., Hidy, G., and Furiness, C.: Comparison of scientific findings from major ozone field studies in North America and Europe, Atmos. Environ., 34, 1885–1920, 2000.

Song, Y., Tang, X. Y., Zhang, Y. H., Hu, M., Fang, C., Zeng, L. M., and Wang, W.: Effects on fine particles by the continued high temperature weather in Beijing, Environ. Sci., 23, 33–36, 2002 (in Chinese).

Stauffer, D. R. and Seaman, N. L.: Use of four-dimensional data assimilation in a limited-area mesoscale model, Part I: Experiments with synoptic-scale data, Mon. Weather Rev., 118, 1205–1277, 1990.

State Environmental Protection Administration of China: China National Environmental Protection Standard: Automated Methods for Ambient Air Quality Monitoring, China Environmental Science Press, Beijing, 2006.

Streets, D. G.: An inventory of gaseous and primary aerosol emission in Asia in the year 2000, J. Geophys. Res., 108, 8809, doi:10.1029/2002JD003093, 2003.

Tang, G., Li, X., Wang, Y., Xin, J., and Ren, X.: Surface ozone trend details and interpretations in Beijing, 2001–2006, Atmos. Chem. Phys., 9, 8813–8823, doi:10.5194/acp-9-8813-2009, 2009.

Tang, G., Li, X., Wang, X., Xin, J., Hu, B., Wang, L., Ren, Y. F., and Wang, Y.: Effects of Synoptic Type on Surface Ozone Pollution in Beijing, Environ. Sci., 31, 573–578, 2010a (in Chinese).

Tang, G.: Modelling of ozone spatial-temporal distribution in the vicinity of Beijing during Olympics, Ph.D thesis, Chinese Academy of Sciences, 153 pp., 2010b.

Tang, X., Li, J., and Danhua, C.: Summertime Photochemical Pollution in Beijing, Pure Appl. Chem., 67, 1465–1468, 1995.

van der A, R. J., Peters, D. H. M. U., Eskes, H. J., Boersma, K. F., Roozendael, M. V., Smedt, I. D., and Kelder, H. M.: Detection of the trend and seasonal variation in tropospheric NO_2 over China, J. Geophys. Res., 111, D12317, doi:10.1029/2005JD006594, 2006.

van der A, R. J., Eskes, H. J., Boersma, K. F., van Noije, T. P. C., Roozendael, M. V., Smedt, I. D., Peters, D. H. M. U., Kuenen, J. J. P., and Meijer, E. W.: Trends, seasonal variability and dominant NO_x source derived from a ten year record of NO_2 measured from space, J. Geophys. Res., 113, D04302, doi:10.1029/2007JD009021, 2008.

van den Hurk, B. J. J. M., Viterbo, P., and Los, S. O.: Impact of leaf area index seasonality on the annual land surface evaporation in a global circulation model, J. Geophys. Res., 108, 4191–4199, doi:10.1029/2002JD002846, 2003.

Wang, X., Zhang, Y., Hu, Y., Zhou, W., Lu, K., Zhong, L., Zeng, L., Shao, M., Hu, M., and Russell, A. G.: Process analysis and sensitivity study of regional ozone formation over the Pearl River Delta, China, during the PRIDE-PRD2004 campaign using the Community Multiscale Air Quality modeling system, Atmos. Chem. Phys., 10, 4423–4437, doi:10.5194/acp-10-4423-2010, 2010.

Wang, T., Wei, X. L., Ding, A. J., Poon, C. N., Lam, K. S., Li, Y. S., Chan, L. Y., and Anson, M.: Increasing surface ozone concentrations in the background atmosphere of Southern China, 1994–2007, Atmos. Chem. Phys., 9, 6217–6227, doi:10.5194/acp-9-6217-2009, 2009.

Wang, Y., McElroy, M. B., Munger, J. W., Hao, J., Ma, H., Nielsen, C. P., and Chen, Y.: Variations of O_3 and CO in summertime at a rural site near Beijing, Atmos. Chem. Phys., 8, 6355–6363, doi:10.5194/acp-8-6355-2008, 2008.

Wang, Y., Hao, J., McElroy, M. B., Munger, J. W., Ma, H., Chen, D., and Nielsen, C. P.: Ozone air quality during the 2008 Beijing Olympics: effectiveness of emission restrictions, Atmos. Chem. Phys., 9, 5237–5251, doi:10.5194/acp-9-5237-2009, 2009.

Wang, Y., Zhang, Y., Hao, J., and Luo, M.: Seasonal and spatial variability of surface ozone over China: contributions from background and domestic pollution, Atmos. Chem. Phys., 11, 3511–3525, doi:10.5194/acp-11-3511-2011, 2011.

Wesely, M.: Parameterization of surface resistances to gaseous dry deposition in regionalscale numerical models. Atmos. Environ., 23, 1293–1304, 1989.

Witte, J. C., Duncun, B. N., Douglass, A. R., Kurosu, T. P., Chance, K., and Retscher, C.: The unique OMI $HCHO/NO_2$ feature during the 2008 Beijing Olympics: Implications for ozone production sensitivity, Atmos. Environ., 45, 3103–3111, 2011.

World Health Organization (WHO): WHO air quality guidelines global update 2005, Bonn, Germany, 30 pp., 2006.

Wongphatarakul, V., Friedlander, S. K., and Pinto, J. P.: A comparative study of $PM_{2.5}$ ambient aerosol chemical databases. Environ. Sci. Technol., 32, 3926–3934, 1998.

Xin, J., Wang, Y., Tang, G., Wang, L., Sun, Y., Wang, Y. H., Hu, B., Song, T., Ji, D. S., Wang, W. F., Li, L., and Liu, G. R.: Variability and reduction of atmospheric pollutants in Beijing and its surrounding area during the Beijing 2008 Olympic Games, Chinese Sci. Bull., 55, 1937–1944, 2010.

Xu, W. Y., Zhao, C. S., Ran, L., Deng, Z. Z., Liu, P. F., Ma, N., Lin, W. L., Xu, X. B., Yan, P., He, X., Yu, J., Liang, W. D., and Chen, L. L.: Characteristics of pollutants and their correlation to meteorological conditions at a suburban site in the North China Plain, Atmos. Chem. Phys., 11, 4353–4369, doi:10.5194/acp-11-

4353-2011, 2011.

Xu, X., Lin, W., Wang, T., Yan, P., Tang, J., Meng, Z., and Wang, Y.: Long-term trend of surface ozone at a regional background station in eastern China 1991–2006: enhanced variability, Atmos. Chem. Phys., 8, 2595–2607, doi:10.5194/acp-8-2595-2008, 2008.

Xu, X. D., Shi, X. H., Xie, L. A., Ding, G. A., Miao, Q. J., Ma, J. Z., and Zheng, X. D.: Spatial character of the gaseous and particulate state compound correction of urban atmospheric pollution in winter and summer, Sci. China Ser. D-Earth Sci., 35(Suppl I), 53–65, 2005.

Yin, D. Z. and Hong, Z. X.: Study on the boundary layer structure and parameters under heavy pollution conditions in Beijing, Clim. Environ. Res., 4, 303–307, 1999 (in Chinese).

Yuval and Broday, D. M.: High-resolution spatial patterns of long-term mean concentrations of air pollutants in Haifa Bay area, Atmos. Environ., 40, 3653–3664, 2006.

Zhang, J., Miao, H., Ouyang, Z. Y., and Wang, X. K.: Ambient air quality trends and driving factor analysis since 1980 in Beijing, J. Environ. Sci.-China, 26, 1886–1892, 2006.

Zhang, Q., Streets, D. G., Carmichael, G. R., He, K. B., Huo, H., Kannari, A., Klimont, Z., Park, I. S., Reddy, S., Fu, J. S., Chen, D., Duan, L., Lei, Y., Wang, L. T., and Yao, Z. L.: Asian emissions in 2006 for the NASA INTEX-B mission, Atmos. Chem. Phys., 9, 5131–5153, doi:10.5194/acp-9-5131-2009, 2009.

Zhang, Y. H., Shao, K. S., Tang, X. Y., and Li, J. L.: The Study of Urban Photochemical Smog Pollution in China, Journal of Natural Science of Peking University, 34, 392–400, 1998.

Zhang, Y. H., Su, H., Zhong, L. J., Cheng, Y. F., Zeng, L. M., Wang, X. S., Xiang, Y. R., Wang, J. L., Gao, D. F., Shao, M., Fan, S. J., and Liu S. C.: Regional ozone pollution and observation-based approach for analyzing ozone-precursor relationship during the PRIDE-PRD2004 campaign, Atmos. Environ., 42, 6203–6218, 2008.

Zheng, J., Zhong, L., Wang, T., Louie, Peter K. K., and Li, Z. C.: Ground-level ozone in the pearl River Delta region: Analysis of data from a recently established regional air quality monitoring network, Atmos. Environ., 44, 814–823, 2010.